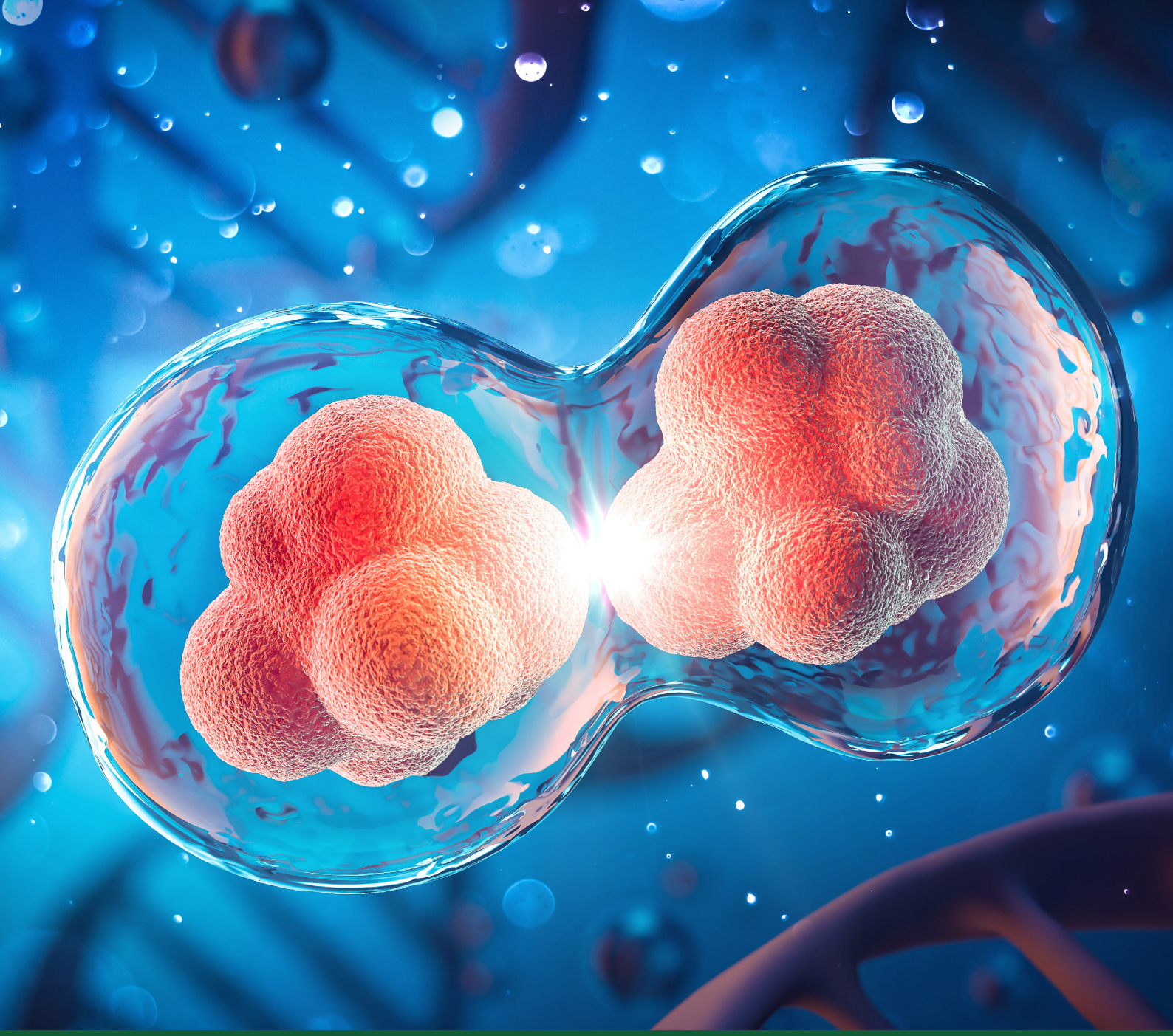

Stem Cells in Focus:

Leveraging the Power of Flow Cytometry

Expert Insights

Sponsored by

BIO-RAD

CURRENT PROTOCOLS
A Wiley Brand

WILEY

Contents

Introduction

Flow cytometry has become a cornerstone technique in stem cell research, providing a window into the cellular and molecular properties that define stem cells. Its versatility in detecting and quantifying a wide array of biological parameters has enabled significant advancements in the isolation, characterization, and understanding of stem cells and their potential applications. As technology continues to evolve, the integration of flow cytometry with other cutting-edge techniques will undoubtedly continue to propel the field of stem cell research forward, opening new avenues for scientific discovery and therapeutic innovation. As the demand for targeted and personalized medical interventions grows, flow cytometry stands at the forefront, enabling the isolation and analysis of specific stem cell subsets. This progress is reshaping the landscape of stem cell research, propelling the development of tailored therapies that address the complex needs of individual patients and their unique cellular profiles, thus steering away from the traditional generalized treatment paradigms.

Flow cytometry is an indispensable technology in the realm of cellular biology, and its application in stem cell research has been transformative. Stem cells, with their unique ability to differentiate into various cell types, hold immense potential for regenerative medicine, disease modeling, and therapeutic interventions. Flow cytometry, with its precise analysis and sorting capabilities, has become an indispensable tool in stem cell research. Together with other techniques, such as molecular assays (e.g., RT-PCR for gene expression), immunocytochemistry, and functional assays, it is crucial for a comprehensive understanding of stem cell characteristics, thereby advancing our knowledge and application of these remarkable cells.

Stem cells are characterized by their dual capacity for self-renewal and differentiation. This means they can proliferate without losing their potency and can also give rise to specialized cell types, a process that is vital for tissue development, maintenance, and repair. There are various types of stem cells, including embryonic stem cells (ESCs), which can differentiate into all cell types of the body, and adult stem cells, such as hematopoietic stem cells (HSCs), which have a more limited differentiation potential. Understanding and harnessing these properties requires sophisticated tools for identifying, isolating, and characterizing stem cells at different stages of their development.

Flow cytometry is a powerful analytical tool that passes thousands of cells per second through a laser beam, measuring multiple physical and chemical characteristics of each cell. It detects fluorescence emitted from dyes or antibodies bound to specific cell components, allowing researchers to identify and quantify various cell populations based on surface markers, intracellular proteins, or other biomolecules. This rapid, multiparametric analysis is particularly useful in stem cell research, where identifying and isolating pure populations of stem cells or their progeny is crucial for both basic research and clinical applications.

One of the primary uses of flow cytometry in stem cell research is the identification and isolation of stem cell subpopulations. Stem cells express particular sets of surface markers that distinguish them from differentiated cells. By using fluorescently labeled antibodies that bind to these markers, scientists can use flow cytometry to identify stem cells within a mixed cell population. Beyond identification, flow cytometry is also used to sort live stem cells based on their surface markers. This sorting capability is essential for obtaining pure populations of stem cells for further study or therapeutic use. The sorted cells can be used in various applications.

Flow cytometry also plays a crucial role in assessing the pluripotency and differentiation potential of stem cells. By measuring the expression of transcription factors and other intracellular molecules associated with pluripotency or specific lineage markers, researchers can determine the state of stem cells and monitor their differentiation into various cell types. This is particularly important in the development of stem cell-based therapies, where the goal is to produce specific cell types that can replace damaged or diseased tissue.

Moreover, flow cytometry is instrumental in evaluating the cell cycle status and viability of stem cells. The ability to analyze DNA content and cell cycle-specific proteins allows researchers to assess the proliferative capacity of stem cells and their progeny, which is vital for understanding their growth dynamics and potential for

long-term tissue maintenance. Additionally, assays for apoptosis and necrosis help in studying the mechanisms of stem cell survival and death, which are crucial for maintaining tissue homeostasis and preventing tumorigenesis.

The two studies highlighted in this Expert Insights eBook exemplify the use of flow cytometry in stem cell research and underscore its potential in uncovering new therapeutic strategies for regenerative medicine.

The first study by Xiaobin Han and Zhongjie Sun [1] investigates the regenerative potential of adult mouse kidney Sca1$^+$ Oct4$^+$ stem/progenitor cells. These cells have been shown to possess the remarkable ability to generate kidney organoids, complex structures that mimic the organization and function of a kidney. Through the use of flow cytometry, these Sca1$^+$ Oct4$^+$ cells were isolated and characterized, revealing their capacity to form kidney-like structures including podocytes, proximal tubules, and capillary networks. This work provides the first evidence that adult kidney stem cells can be coaxed in vitro to form complex organoids, opening new avenues for the development of organoid-based therapies for kidney failure.

The second study by Kunchi Zhao and colleagues [2] delves into the role of microRNA-125b (miR-125b) in the context of spinal cord injury (SCI), a devastating condition with limited therapeutic options. Flow cytometry was instrumental in identifying and analyzing neural stem cells (NSCs) affected by miR-125b expression. The study found that manipulating miR-125b levels in spinal cord injury rat models and neural stem cells affects neural regeneration, with inhibition leading to protein changes that impede recovery, and overexpression promoting neurological function and favorable protein expression, linked to the miR-125b regulation of the Smurf1-KLF2-ATF2 pathway. These findings suggest a therapeutic potential for miR-125b overexpression in enhancing recovery after SCI by modulating molecular pathways critical for neural stem cell survival and differentiation.

These two research papers highlight the versatility of flow cytometry in stem cell research, providing insights into stem cell biology and offering hope for new treatments. By facilitating the isolation and characterization of specific cell populations, flow cytometry becomes an essential tool in understanding the molecular cues that govern stem cell fate and function. As researchers continue to unravel the complexities of stem cell behavior and their environment, the integration of flow cytometry with other advanced techniques will undoubtedly contribute to the development of novel regenerative therapies.

In the last part of our eBook, we explore the potential of high-throughput analysis in the context of rare event detection, a crucial aspect of applications such as stem cell research. We reveal how the **ZE5 Cell Analyzer** maintains accurate detection rates of up to 100,000 events per second without data loss or compromised resolution. This capability not only ensures the integrity of rare event analysis but also significantly cuts down on the time required for data acquisition. The eBook concludes with a concise summary of three case studies in which the ZE5 Cell Analyzer has been utilized in stem cell research, as well as a further reading section with links to additional research articles.

References

[1] Han, X., & Sun, Z. (2022). Adult Mouse Kidney Stem Cells Orchestrate the *De Novo* Assembly of a Nephron via Sirt2-Modulated Canonical Wnt/β-Catenin Signaling. Advanced Science, 9(15), e2104034. https://doi.org/10.1002/advs.202104034.

[2] Zhao, K., Li, R., Ruan, Q., Meng, C., Yin, F., & Zhu, Q. (2021). microRNA-125b and its downstream Smurf1/KLF2/ATF2 axis as important promoters on neurological function recovery in rats with spinal cord injury. Journal of Cellular and Molecular Medicine, 25(13), 5924–5939. https://doi.org/10.1111/jcmm.16283.

Adult Mouse Kidney Stem Cells Orchestrate the *De Novo* Assembly of a Nephron via Sirt2-Modulated Canonical Wnt/β-Catenin Signaling

Adapted from Xiaobin Han and Zhongjie Sun

Adult mouse kidney Sca1⁺ Oct4⁺ stem/progenitor cells can generate kidney organoids, indicating their regenerative potential. These cells form kidney-like structures, including podocytes, proximal tubules, and capillary networks. In 3D and monolayer cultures, they differentiate into mature tubules and nephron-like structures that functionally endocytose dextran. The process relies on Sirt2-mediated Wnt/β-catenin signaling. This study provides the first evidence that adult mouse kidney stem cells can generate complex kidney organoids *de novo*, offering promising insights for treating kidney failure through organoid-based therapies.

Introduction

Studies over the past decade have reported the presence of stem cells in adult mammalian kidneys using markers such as Sca1, CD45, and CD133, although no definitive kidney organoids have been generated from these cells, leaving the existence of adult kidney stem cells (KSCs) debated. This study employed a novel approach for isolating KSCs from adult mouse kidneys using Sca1 and Oct4 markers, resulting in cells also expressing CD133, CD34, CD45, and renal markers like cadherin-11, WT-1, Pax-2, and Wnt4. These Sca1⁺ Oct4⁺ cells can form kidney organoids in culture, integrating Wnt signaling and SIRT2 modulation to develop glomerular structures with vascular networks and functional nephron-like structures. This methodology offers insights into kidney development and potential avenues for personalized kidney regeneration.

Results

Isolation of Sca1⁺ Oct4⁺ Cells from Adult Mouse Kidney

To isolate KSCs, single cells from collagenase II-digested adult mouse kidneys (without injury) were cultured in a sequence of media (Figure 1): initial 24-hour serum-free Medium A, followed by ≤7-day Medium B, and then up to 6 weeks in Medium C to recover stem/progenitor cells. (See full publication for media compositions.) Stem cell antigen-1 positive (Sca1⁺) cells were isolated and purified, resulting in ~97% Sca1⁺ Oct4⁺ cells. These cells also expressed hematopoietic markers CD133, CD45, CD34, and renal markers Pax-2, WT-1, cadherin-11, and Wnt4. Sca1⁺ Oct4⁺ cells formed 3D kidney organoids overnight, growing to >300 μm within 14 days, and retained organoid-forming ability over 2.5 years across >150 passages.

Sca1⁺ Oct4⁺ Cell-Derived Kidney Organoids Contain Glomerular-Like Structures with a *De Novo* Vascular Network

To investigate kidney organoid development, organoid growth and gene expression were analyzed over time (Figure 2). By day 3, organoids reached ~80 μm in diameter, expanding to ~400 μm by day 14. Key kidney developmental genes, including LHX1, GATA3, HOXD11, EYA1, and TBX6, were upregulated from day 0 to 14, while presomitic mesoderm (PSM) marker T was downregulated. Podocyte markers WT-1 and nephrin increased, with no significant change in Wnt4 expression, which was initially high in Sca1⁺ Oct4⁺ cells. The organoids differentiated in Medium C and APEL medium formed kidney-like structures, including cortex, medulla, renal column, and renal capsule. Cryosection staining identified glomerulus-like structures with nephrin⁺ cells, tubular markers, podocytes, and endothelial cells. This development of isolated Sca1⁺ Oct4⁺ cells into self-organized 3D organoids with upregulated expression of kidney developmental genes provides supporting evidence that they are KSCs. These findings also suggest that these differentiated Sca1⁺ Oct4⁺ cell-derived organoids contain endothelial (CD31⁺), podocyte (nephrin⁺), and distal tubular (NCC⁺) lineages.

Figure 1

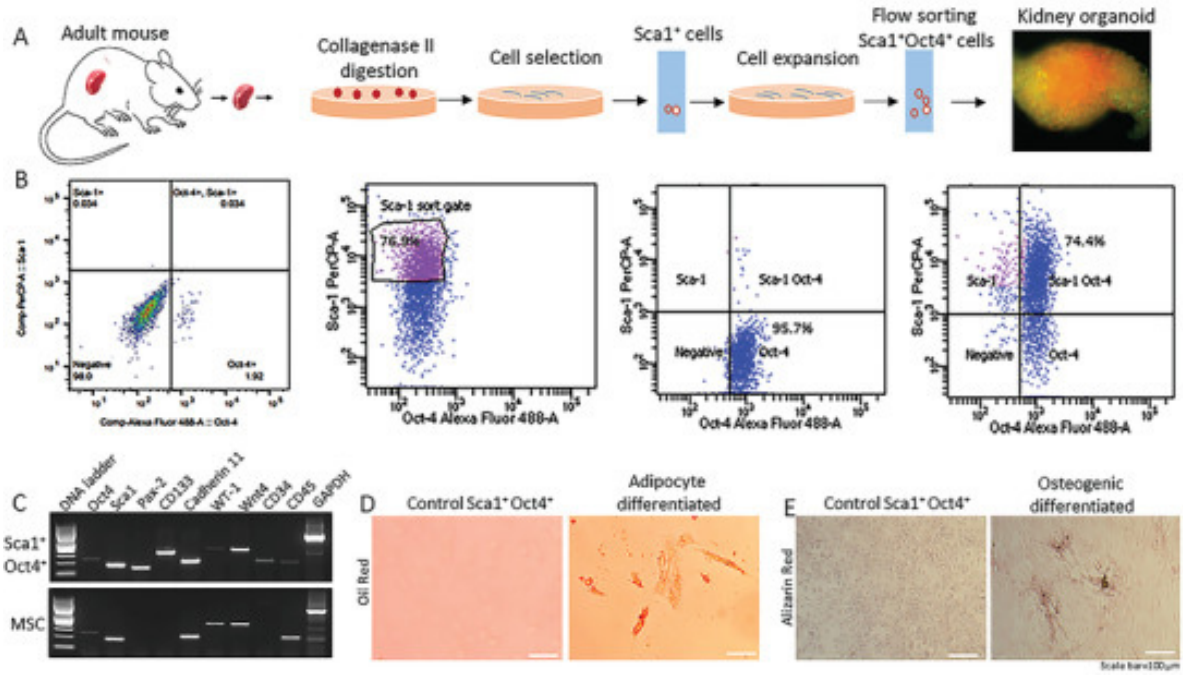

The isolated Sca1+ Oct4+ cells form self-organizing organoids. A) Workflow for isolation of Sca1+ Oct4+ cells. B) Purification of Sca1+ cells by flow cytometry using a Bio-Rad ZE5 Cell Analyzer and confirmation of Sca1+ Oct4+ expression by double antibody labeling. C) RT-PCR analysis of stem cell and renal markers in mouse mesenchymal stromal cells (MSCs) versus isolated Sca1+ Oct4+ cells. D) Adipocyte differentiation of Sca1+ Oct4+ cells. Scale bar, 100 µm. E) Osteogenic differentiation of Sca1+ Oct4+ cells. Scale bar, 100 µm. Data are representative of three independent experiments.

Figure 2

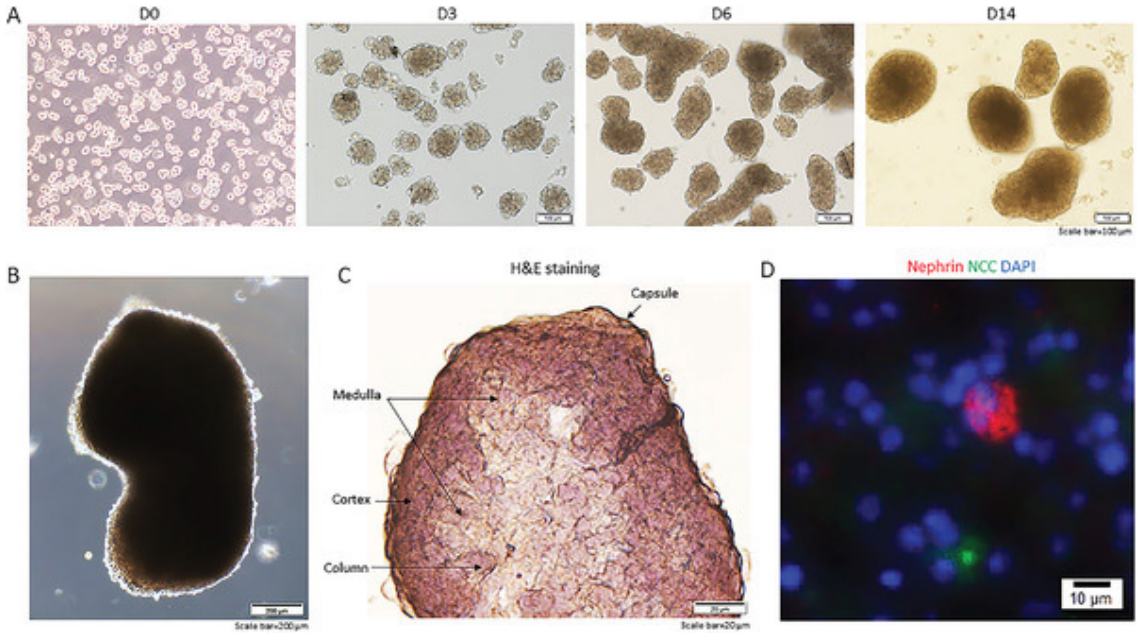

Kidney organoids derived from isolated Sca1+ Oct4+ cells develop kidney structures and glomerular lineage. A) Time course of the development of Sca1+ Oct4+ cell derived kidney organoids in culture. Scale bar, 100 µm. B) Bright field of kidney-shaped KSCs derived organoid. Scale bar, 200 µm. C) Cryosection of kidney organoids (H&E staining) revealing kidney structures including cortex, medulla, column, and capsule. Scale bar, 20 µm. D) Cryosections of kidney organoids were further processed with immunofluorescent staining. The photo shows glomerulus-like structure with positive staining for nephrin (red) and distal tubule positive staining for NCC (green, arrow). Scale bar, 10 µm. Data is representative of three independent experiments.

Figure 3

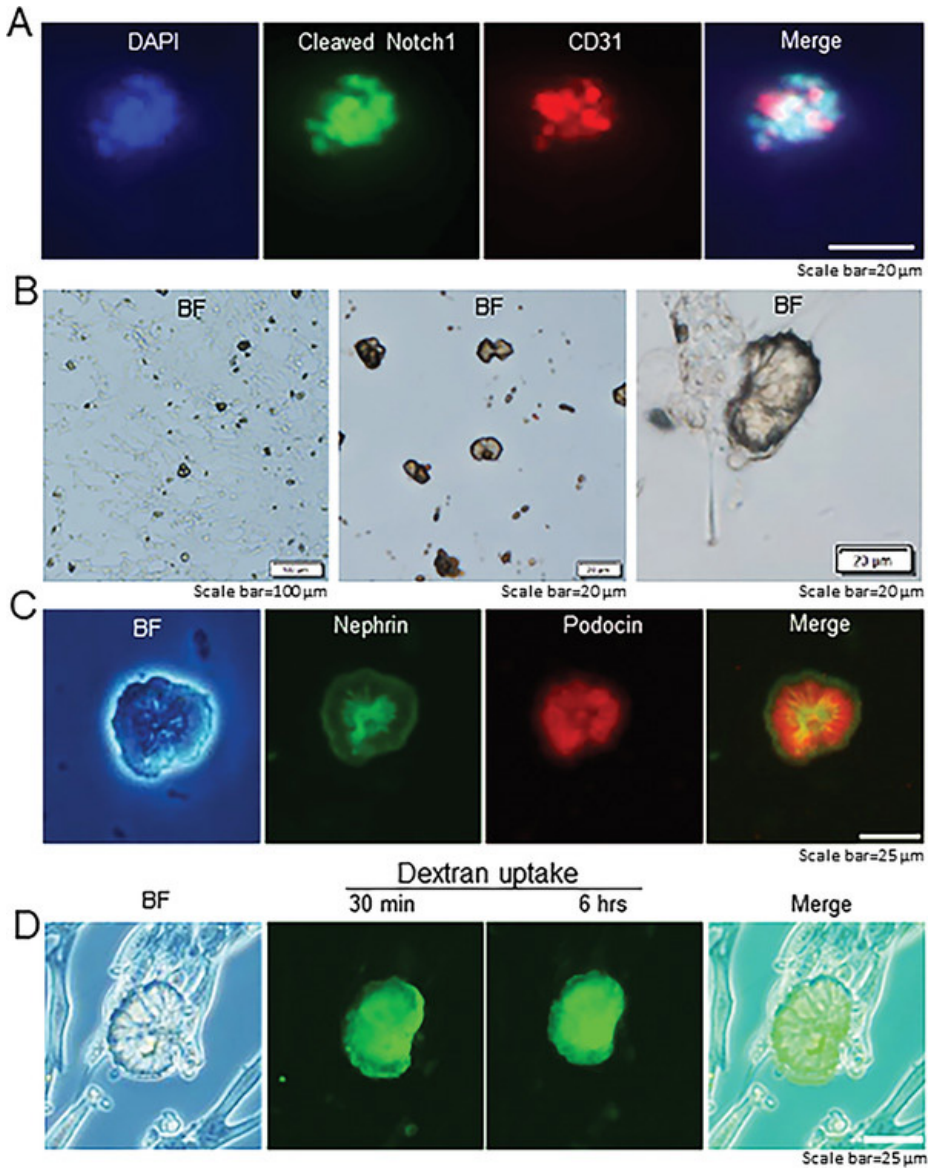

Generation of self-organizing kidney-shaped structures from the differentiated Sca1+ Oct4+ monolayer cultures. A) Comma-shaped body with positive staining of cleaved-Notch1 and CD31. Scale bar, 20 µm. B) Bright field (BF) of differentiation of the isolated Sca1+ Oct4+ cells and subsequent generation of self-organized kidney-shaped structures. Scale bar, 100, 20, and 20 µm. C) Expression of nephrin and podocin in self-organizing kidney shaped structures assembled by differentiated Sca1+ Oct4+ cells. Scale bar, 25 µm. D) Uptake of 70 kDa FITC-dextran by kidney-shaped structures after 30 min and 6 h. Scale bar, 25 µm. Data is representative of three independent experiments.

Monolayer Cultures of Differentiated Sca1$^+$ Oct4$^+$ Cells Reveal Functional Mini Kidney-Like Structure and an Entire *De Novo* Nephron

To characterize Sca1$^+$ Oct4$^+$ cells, differentiation was induced using Medium D for up to 7 days and APEL medium for up to 30 days. Differentiated monolayer cultures showed ureteric bud (GATA3$^+$) cells with surrounding metanephric mesenchyme (Six2$^+$), indicating progenitor cells for collecting ducts and nephrons. Comma- and S-shaped bodies were also observed, signifying early Notch signaling-mediated nephrogenesis (Figure 3). These cells formed kidney-shaped structures expressing podocyte markers nephrin and podocin, and demonstrated dextran uptake, indicating proximal tubule presence.

Further investigation revealed that Sca1⁺ Oct4⁺ cells could generate a ≈2-mm self-organizing nephron over a period of 60 days (Figure 4A). This nephron contained a glomerulus, proximal tubule, and collecting duct. Although the loop of Henle and distal convoluted tubule markers were not fluorescently labeled due to tissue permeability, these lineages were identified in monolayer cultures. Additionally, proximal tubule-like structures were found near S-shaped bodies.

Western blot analysis confirmed the presence of glomerular markers CD31, nephrin, and podocin, with differentiation-associated increases in CD31 and nephrin, and a switch from podocin 1 in undifferentiated cells to podocin 2 in differentiated cells. These findings indicate that Sca1⁺ Oct4⁺ cells can orchestrate the *de novo* generation of nephron and tubular lineages, supporting their classification as KSCs capable of nephrogenesis.

Figure 4

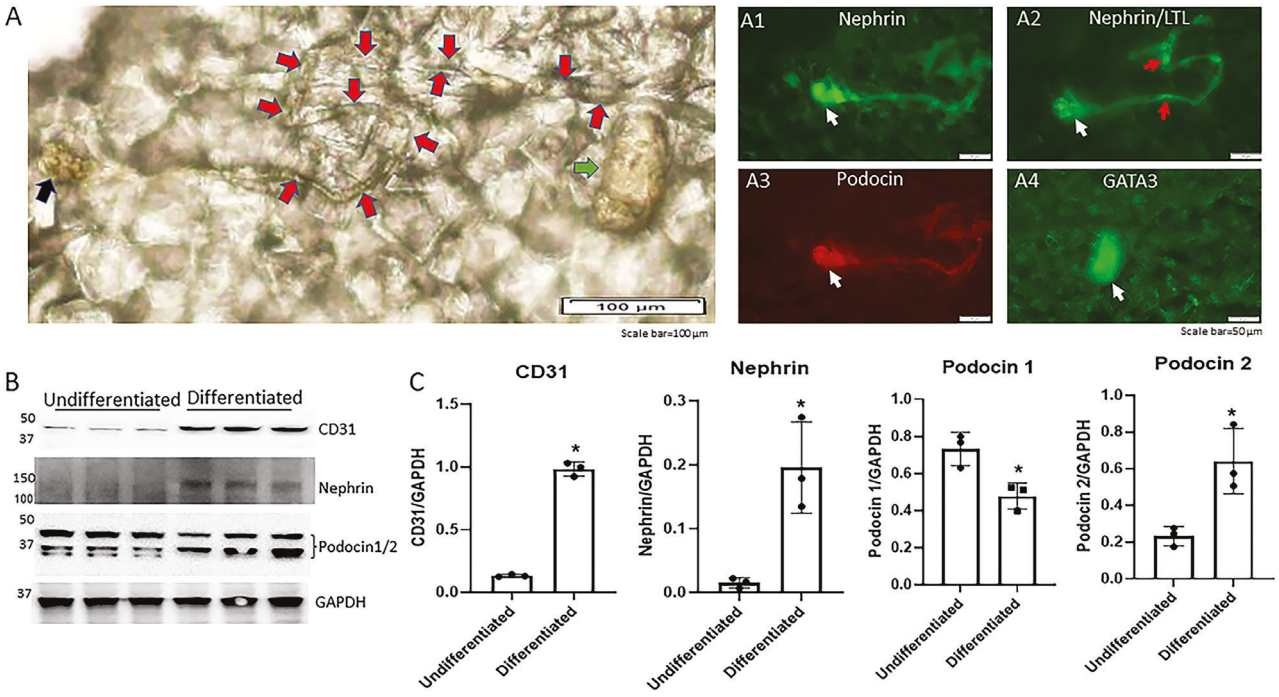

Generation of a self-organizing *de novo* nephron from the differentiated Sca1⁺ Oct4⁺ monolayer cultures. A) Bright field image of self-organizing organoid-like structure from monolayer culture of KSCs. The photo shows glomerulus-like structure (black arrow), tubule-like structure (red arrows), and collecting duct-like structure (green arrow). Scale bar, 100 µm. A1) Glomerulus-like structure stained with nephrin (white arrow). Scale bar, 50 µm. A2) Glomerulus-like structure stained with nephrin (white arrow) and proximal tubule-like structure stained with LTL (red arrows). Scale bar, 50 µm. A3) Glomerulus-like structure stained with podocin (white arrow). Scale bar, 50 µm. A4) Collecting duct-like structure stained with GATA3 (white arrow). Scale bar, 50 µm. C) Western blot analysis of CD31, nephrin, and podocin expression in undifferentiated and differentiated Sca1⁺ Oct4⁺ cells. GAPDH was used as a loading control. Data is representative of three independent experiments. Values represent the mean ± SD (n = 3). $p < 0.05$ versus control by 2-tailed Student's t test.

Sirt2 Modulates Canonical Wnt/β-Catenin Signaling During Kidney Organoid Development

To investigate how Sca1⁺ Oct4⁺ KSCs form kidney organoids and *de novo* nephrons, the authors analyzed canonical Wnt/β-catenin signaling dynamics (Figure 5). The data revealed a biphasic Wnt signaling pattern: high in stem cells, reduced in early organoid formation, and reactivated by day 14. Conversely, GSK3β, a Wnt signaling inhibitor, showed decreased expression during organoid development. Sirt2 expression was low initially (days 0-6) but significantly increased by day 14, mirroring the expression of podocyte marker podocin. Sirt2 knockdown disrupted Wnt signaling and organoid formation, reducing podocin levels. This suggests Sirt2's critical role in modulating Wnt signaling for kidney organoid development. A schematic developmental model of KSC-derived kidney organoid labeled with mCherry/GFP is illustrated in Figure 6. Finally, Sirt1 and Sirt3 expressions were downregulated, indicating they are not essential in this process.

Figure 5

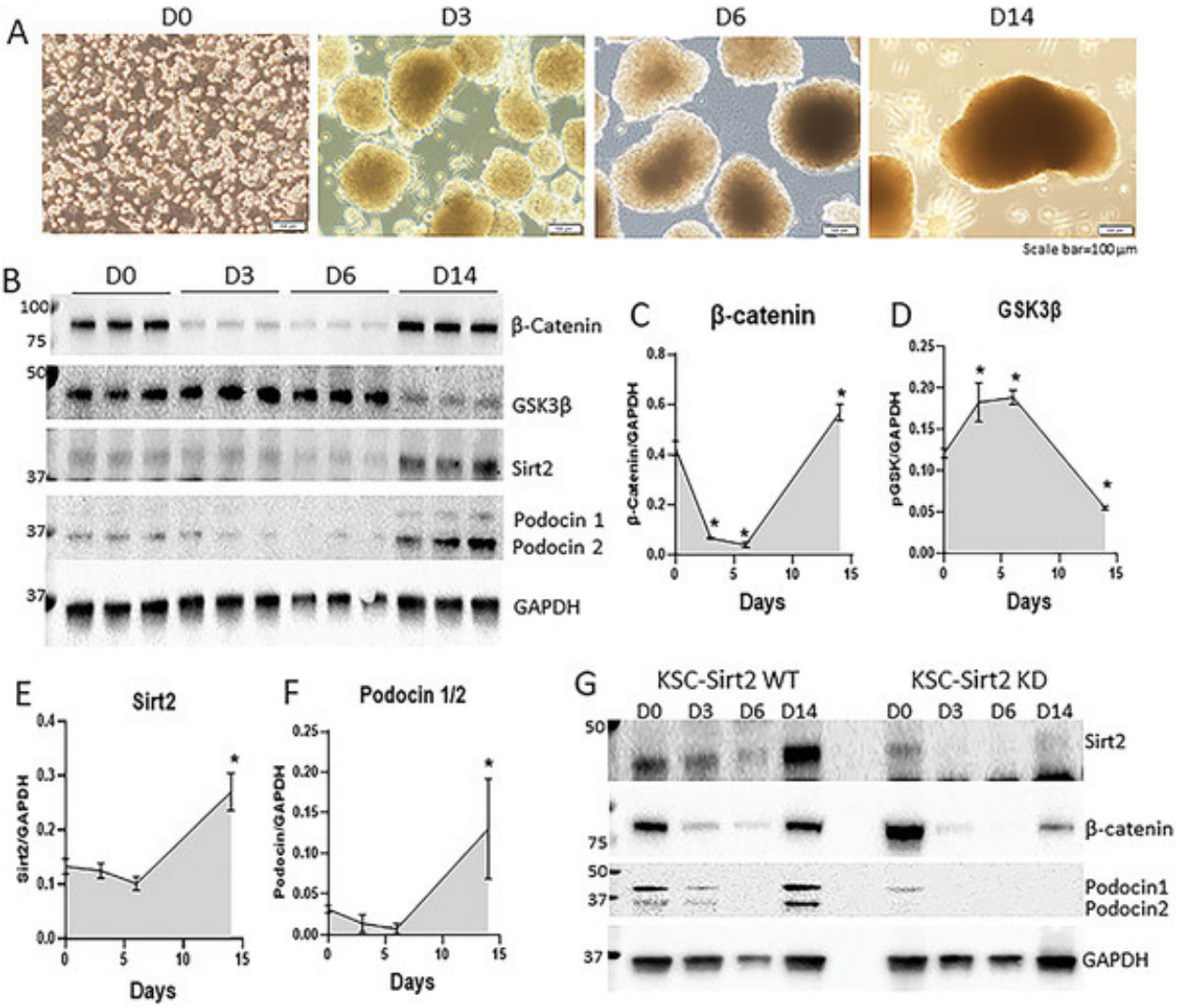

Sirt2 is required for dynamic change of canonical Wnt/β-catenin signaling during kidney organoid development. A) Model of self-organized kidney organoid development from single KSCs. Scale bar, 100 μm. B) Western blot analysis of expression of β-catenin, GSK3β, Sirt2, and podocin1/2 during kidney organoid development. GAPDH was used as loading control for quantitation. C–F) Quantification of gene expression for β- catenin, GSK3β, Sirt2, and podocin1/2, respectively. G) Western blot analysis of Sirt2, β-catenin, and podocin1/2 in KSC-Sirt2 wt or KSC-Sirt2 knockdown (KD) kidney organoids. *p < 0.05 versus day 0.

Figure 6

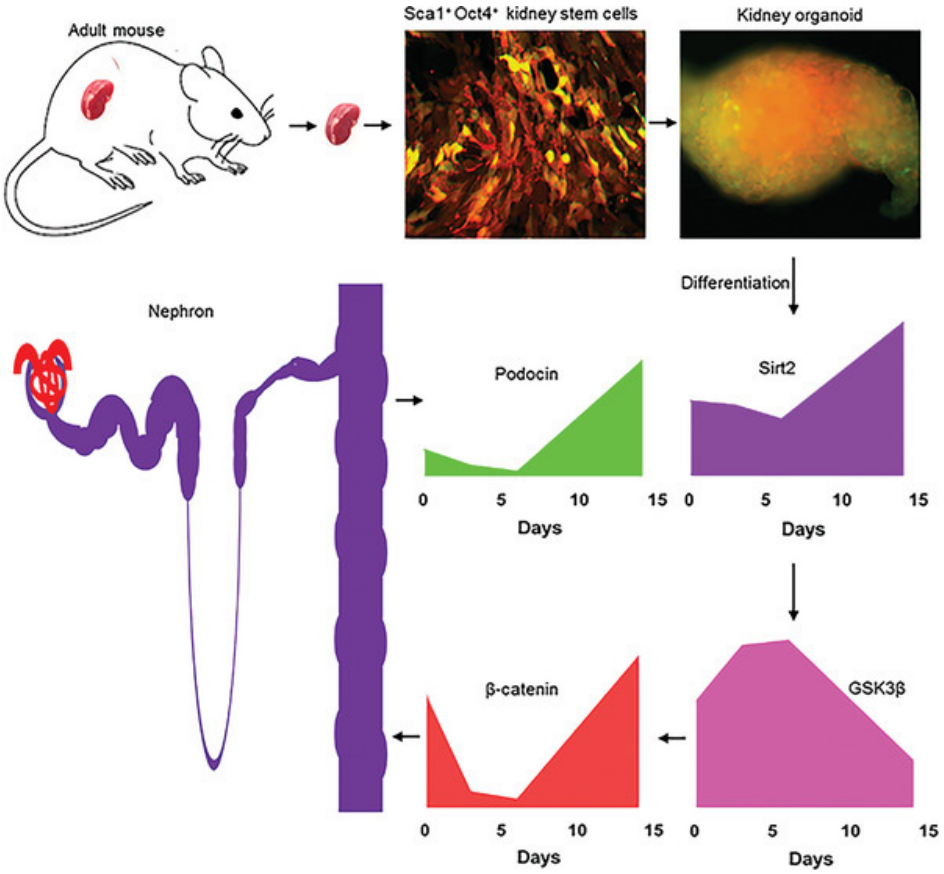

Schematic model of Sirt2-mediated development of adult KSC-derived kidney organoids. Adult KSCs reside in the mouse kidney. KSCs were isolated using Sca1/Oct4 selection markers and labeled with mCherry and CD63-GFP. KSCs formed self-organized kidney organoid in culture mediated by Sirt2 expression. Sirt2 regulates GSK3β activity leading to a dynamic change of canonical Wnt/β-catenin signaling and promotes the formation of KSCs-derived kidney organoid and nephron development.

Discussion

KSCs and derived kidney organoids offer novel insights into kidney development and potential applications in precision medicine. This study provides evidence supporting the presence of stem cells in adult mouse kidneys. KSCs were shown to express common stem cell and renal markers, form 3D kidney organoids with glomerular structures, and differentiate into kidney-shaped structures with nephrin and podocin markers, demonstrating functional characteristics such as selective dextran endocytosis. Comma- and S-shaped bodies observed during differentiation indicate active Notch signaling, essential for nephrogenesis. Notably, nephron structures were generated *de novo* from KSC-derived monolayer cultures.

Unlike previous methods using human pluripotent stem cells, this new approach revealed endogenous self-regulation of canonical Wnt signaling during organoid development, exhibiting a biphasic pattern—high in stem cells, reduced in early stages, and reactivated by day 14. This dynamic signaling is crucial for nephron formation. Sirt2, whose expression increased in tandem with podocin, modulated Wnt signaling, with its knockdown impairing organoid development and podocin expression.

While these findings confirm that Sirt2 and Wnt signaling play pivotal roles in KSC-derived kidney organoid formation, the study primarily achieved glomerulus-like structures with limited nephron tubular segments. Future research should focus on enhancing 3D culture techniques to improve nephron development and exploring KSC applications in kidney disease models. This study advances our understanding of kidney development and organoid generation, providing a framework for further exploration in kidney regenerative medicine.

microRNA-125b and its Downstream Smurf1/KLF2/ATF2 Axis as Important Promoters on Neurological Function Recovery in Rats with Spinal Cord Injury

Adapted from Kunchi Zhao, Ran Li, Qing Ruan, Chunyang Meng, Fei Yin, and Qingsan Zhu

This study explored the role of microRNA-125b (miR-125b) in spinal cord injury (SCI) and its interaction with Smurf1, a ubiquitin ligase, and other proteins. Using loss- and gain-of-function methods in SCI rat models and neural stem cells (NSCs), researchers found that inhibiting miR 125b led to the up-regulation of Smurf1 and activating transcription factor-2 (ATF2), while overexpressing miR-125b improved neurological function. This was evidenced by elevated Basso-Beattie-Bresnahan scores and increased expression of proteins like Nestin and Bcl-2, with reduced Bax expression and cell apoptosis. Smurf1, targeted by miR-125b, facilitated the degradation of Krüppel-like factor 2 (KLF2), which in turn suppressed ATF2 expression in NSCs. These findings suggest that miR-125b overexpression promotes recovery after SCI by modulating these molecular pathways.

Introduction

Spinal cord injury (SCI), predominantly resulting from accidents, falls, and violence, leads to significant neurological damage, especially in the elderly. In China, SCI affects the physiological, psychological, and social well-being of 60,000 people per year. Current treatments aim to promote neurological recovery and mitigate secondary damage, with cell transplantation being a promising approach. However, no therapies specifically target the neurological deficits caused by SCI, emphasizing the need to understand the underlying mechanisms.

Research indicates that altering microRNA (miR) levels can influence neurological outcomes. miR-125b, which is highly expressed in the brain and other tissues, has shown potential in promoting neurological recovery in SCI rats. Bioinformatics analysis identifies Smad ubiquitylation regulatory factor-1 (Smurf1) as a target of miR-125b. Smurf1, an E3 ubiquitin ligase, can induce neuronal necroptosis and degrade Krüppel-like factor 2 (KLF2), which provides neuroprotection by modulating the blood-brain barrier and reducing inflammation. KLF2 also suppresses activating transcription factor-2 (ATF2), further reducing inflammation. The results of this study suggest that the miR-125b/Smurf1/KLF2/ATF2 axis plays a crucial role in SCI, proposing novel targets for therapeutic intervention.

Results

Overexpression of miR-125b inhibited SCI and promoted the recovery of nerve function in rats

This study investigated the role of miR-125b in spinal cord injury (SCI) using Sprague Dawley (SD) rat models. SCI rats exhibited significantly lower Basso-Beattie-Bresnahan (BBB) scores, indicating impaired motor function, and reduced miR-125b expression compared to normal and sham-operated rats (Figure 1). Histological examination showed severe spinal cord damage in SCI rats, including disordered tissue structure, neuronal degeneration, inflammation, and increased apoptosis, confirmed by TUNEL assay. Protein analysis revealed decreased levels of neural markers (Nestin, NeuN, GFAP, NF-200) and anti-apoptotic Bcl-2, with elevated pro-apoptotic Bax levels, indicating inhibited neuron proliferation and increased apoptosis.

Rats treated with miR-125b agomir showed improved motor function, as reflected by higher BBB scores, and increased miR-125b expression. Histological analysis showed reduced spinal cord pathology, and TUNEL assay indicated decreased apoptosis in these rats. Western blot results demonstrated increased levels of neural markers and Bcl-2, and reduced Bax expression following miR-125b agomir treatment. These findings suggest that miR-125b overexpression can mitigate SCI's pathological effects, enhance neural marker expression, reduce apoptosis, and improve neurological recovery, highlighting miR-125b's therapeutic potential for SCI.

Figure 1

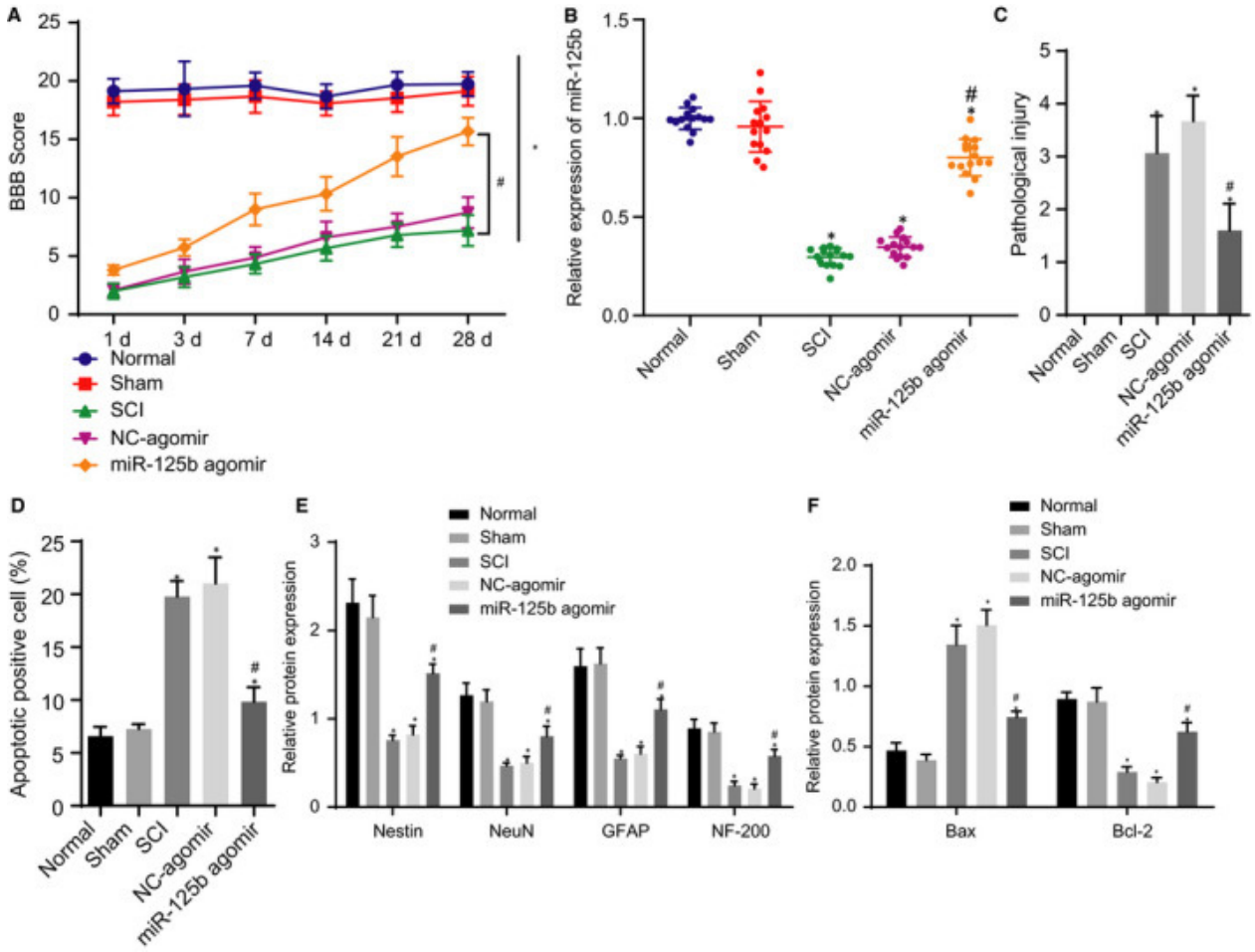

SCI development is repressed and promoted the recovery of nerve function by overexpressing miR-125b in rats. Normal rats and sham-operated rats were used as controls, and SCI rats were treated or not treated with NC-agomir and miR-125b. (A) BBB scores of rats. (B) RT-qPCR detection of miR-125b expression in the injured spinal cord of rats normalized to U6. (C) HE staining analysis of the pathological changes of the spinal cord of rats. (D) Apoptotic-positive cells in the spinal cord of rats detected by TUNEL staining. (E) Western blot analysis of protein expression of Nestin, NeuN, GFAP and NF-200 normalized to GAPDH. (F) Western blot analysis of expression of Bax and Bcl-2 protein normalized to GAPDH. *P < .05 vs sham-operated rats and normal rats, #P < .05 vs SCI rats treated with NC-agomir. Data between the 2 groups were compared by an unpaired t test, and comparisons among multiple groups were performed with one-way ANOVA. Scores at different time-points were compared by repeated measures ANOVA. n = 15 in each group

miR-125b targeted down-regulated Smurf1

Building on the role of miR-125b in SCI, this study aimed to uncover its downstream mechanisms. Using bioinformatics tools (miRDB, TargetScan, miRWalk), 55 potential target genes of miR-125b were identified. Further interaction analysis pinpointed Smurf1 as a key target (Figure 2). A dual-luciferase reporter assay confirmed that miR-125b directly binds to Smurf1's 3'UTR, decreasing luciferase activity, confirming Smurf1 as a target gene.

RT-qPCR and Western blot analyses revealed elevated Smurf1 mRNA and protein levels in SCI rats compared to controls, indicating its role in SCI pathology. Neural stem cells (NSCs), known for their differentiation and migration abilities, were used for further study. Transfecting NSCs with miR-125b mimic increased miR-125b expression and decreased Smurf1 levels, while the opposite occurred with miR-125b inhibitor. These results suggest that miR-125b downregulates Smurf1 in NSCs, highlighting Smurf1's increased expression in SCI and miR-125b's potential in inhibiting it, pointing to a critical regulatory pathway in SCI recovery.

Figure 2

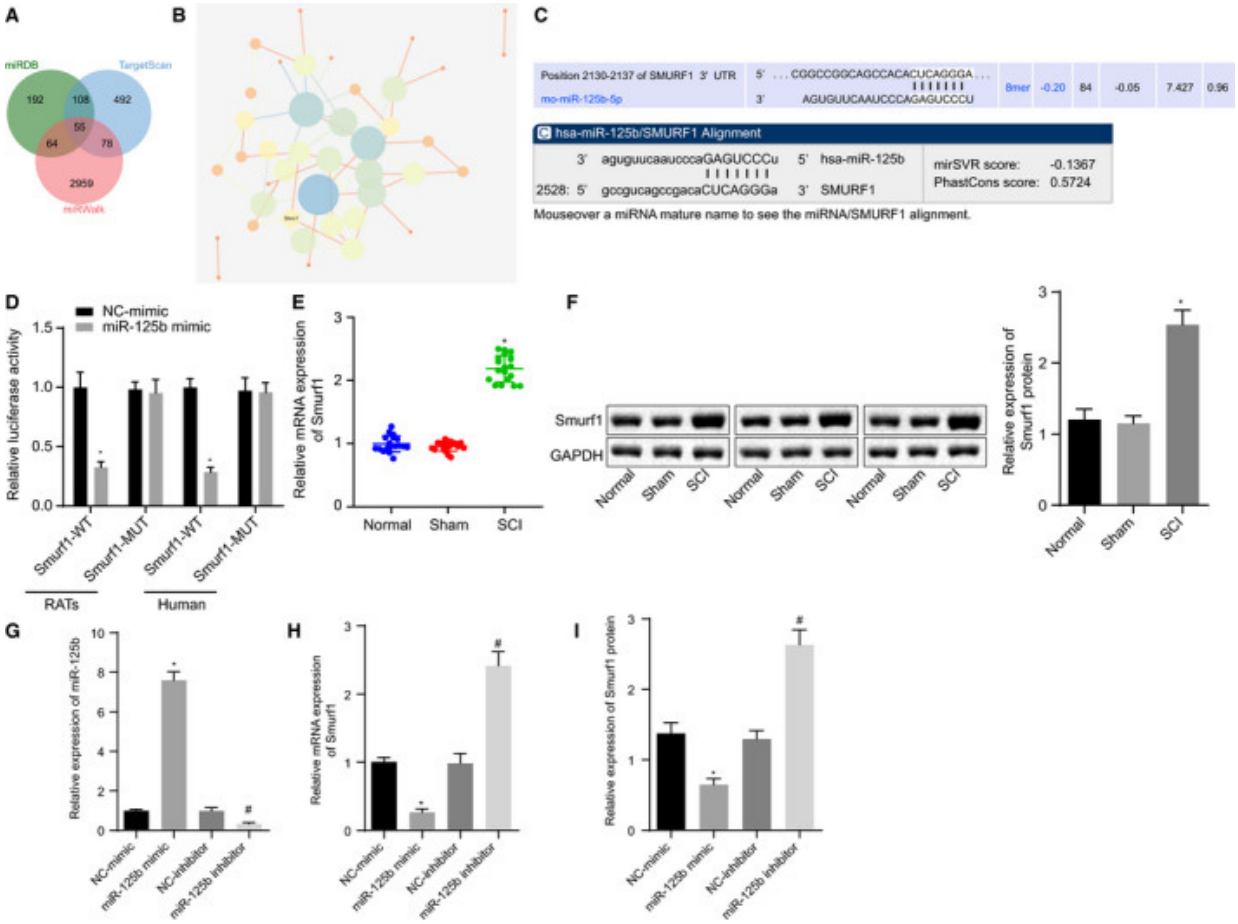

Smurf1 is a target gene of miR-125b in NSCs. (A) A Venn diagram of the intersection of the predicted downstream target genes of miR-125b in miRDB, TargetScan and miRWalk bioinformatics websites. (B) The network of interaction relationship among 55 candidate genes analysed by STRING website. The circles in the figure from large to small represent degree values of genes from large to small, the circle colours from blue to orange represent Degree from large to small, and the lines in the middle of the circles represent co-expression relationships among genes. (C) Binding site between miR-125b and Smurf1 in rats and human predicted by Targetscan and miRanda websites. (D) The targeting relationship between miR-125b and Smurf1 verified by dual-luciferase reporter gene assay. (E) RT-qPCR detection of the expression of Smurf1 in the spinal cord of rats after modelling normalized to GAPDH. (F) Western blot analysis of the expression of Smurf1 protein in the spinal cord after modelling normalized to GAPDH. NSCs were transfected with miR-125b mimic, NC mimic, miR-125b inhibitor and NC inhibitor. (G) Expression of miR-125b in NSCs detected by RT-qPCR normalized to U6. (H) Expression of Smurf1 mRNA in NSCs detected by RT-qPCR normalized to GAPDH. (I) Expression of Smurf1 protein in NSCs detected by Western blot analysis normalized to GAPDH. *P < .05 vs sham-operated rats and normal rats, or the transfection with NC mimic, #P < .05 vs NSCs transfected with NC inhibitor. Data between the two groups were compared by an unpaired t test and comparisons among multiple groups were performed with one-way ANOVA. Rats: n = 15 in each group. The cell experiment was repeated three times.

Overexpression of miR-125b targeted Smurf1 to promote proliferation and migration but inhibit apoptosis in NSCs

To investigate how miR-125b affects NSCs, cells were transfected with miR-125b mimic and Smurf1 overexpression constructs. Results showed increased miR-125b and decreased Smurf1 levels with the miR-125b mimic. Overexpressing Smurf1 did not affect miR-125b levels but increased Smurf1 expression.

NSCs with miR-125b mimic had higher viability and migration abilities and reduced apoptosis, as shown by CCK-8, Transwell, and flow cytometry assays. Flow cytometry was performed using a Bio-Rad ZE5 Cell Analyzer. However, these benefits were reversed when Smurf1 was overexpressed. Adding miR-125b mimic countered the negative effects of Smurf1 overexpression on NSCs. Thus, miR-125b promotes NSC proliferation and migration while inhibiting apoptosis by targeting Smurf1.

Figure 3

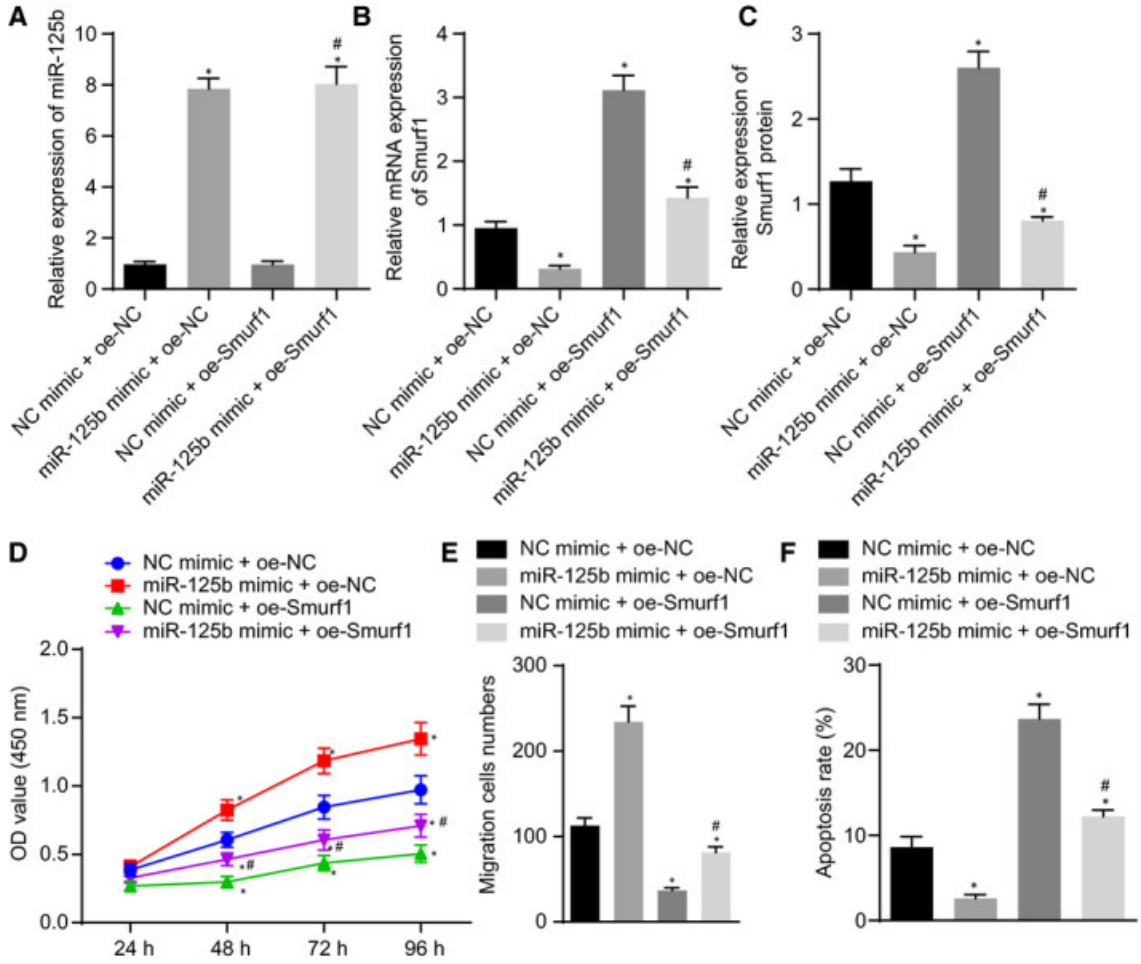

The overexpression (oe) of miR-125b or silencing of Smurf1 induces proliferation and migration but represses apoptosis in NSCs. NSCs were transfected with NC mimic + oe-NC, miR-125b mimic + oe-NC, NC mimic + oe-Smurf1 or miR-125b mimic + oe-Smurf1. (A) Expression of miR-125b in NSCs measured by RT-qPCR normalized to U6. (B) Smurf1 mRNA expression in NSCs measured by RT-qPCR normalized to GAPDH. (C) Expression of Smurf1 protein in NSCs detected by Western blot analysis normalized to GAPDH. (D) NSC viability measured by CCK 8. (E) NSC migration evaluated by Transwell assay. (F) NSC apoptosis assessed by flow cytometry using a Bio-Rad ZE5 Cell Analyzer. *P < .05 vs NSCs transfected with NC mimic + oe-NC, #P < .05 vs NSCs transfected with NC mimic + oe-Smurf1. Comparisons among multiple groups were performed with one-way ANOVA, and cell viability at different time-points was compared using two-way ANOVA. The cell experiment was repeated 3 times.

Smurf1 promoted the degradation of KLF2 through its E3 ubiquitin ligase function

The following experiments examined the effects of KLF2 on Smurf1 expression in SCI. Using the GeneCards database, 1527 proteins interacting with Smurf1 and 1803 SCI-related genes were identified, with 238 genes intersecting both lists. Among these, 27 transcription factors were highlighted, with KLF2 being a key player (Figure 4).

RT-qPCR and Western blot analysis showed significantly lower KLF2 levels in SCI rats compared to normal and sham-operated rats. Pearson's correlation analysis indicated a negative correlation between KLF2 and Smurf1 expression in SCI rats. Co-immunoprecipitation (Co-IP) experiments revealed that Smurf1 and KLF2 directly interact. Overexpressing Smurf1 in NSCs increased Smurf1 mRNA and protein levels but decreased KLF2 levels. Adding the proteasome inhibitor MG132 showed that Smurf1 promoted KLF2 degradation through its E3 ubiquitin ligase activity.

Further, NSCs with overexpressed Smurf1 displayed increased ubiquitination of KLF2, demonstrating that Smurf1 targets KLF2 for degradation. These findings suggest that KLF2 expression is reduced in SCI and that Smurf1 mediates KLF2 degradation, implicating Smurf1 as regulatory factor in SCI pathology.

Figure 4

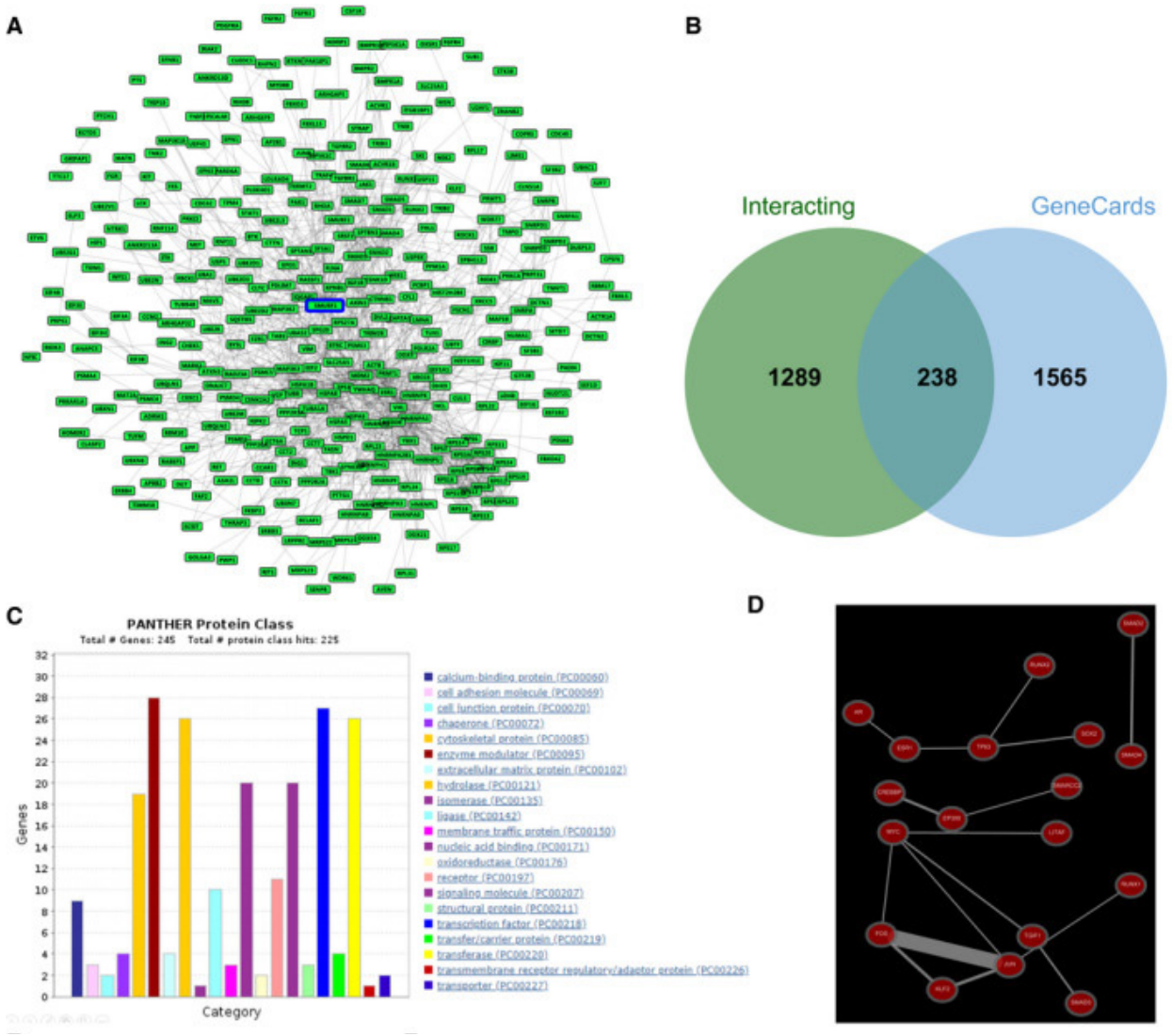

Smurf1 degrades KLF2 via its E3 ubiquitin ligase function. (A) Interacting proteins of Smurf1 gene in GeneCards database. (B) Venn diagram of intersection of interacting proteins of Smurf1 gene in GeneCards database and SCI-related genes. (C) Classification of coding proteins of genes by Panther website. (D) Co-expression network of transcription factors in Coexpedia database. *Figure and legend continued on next page.*

Figure 4 (cont.)

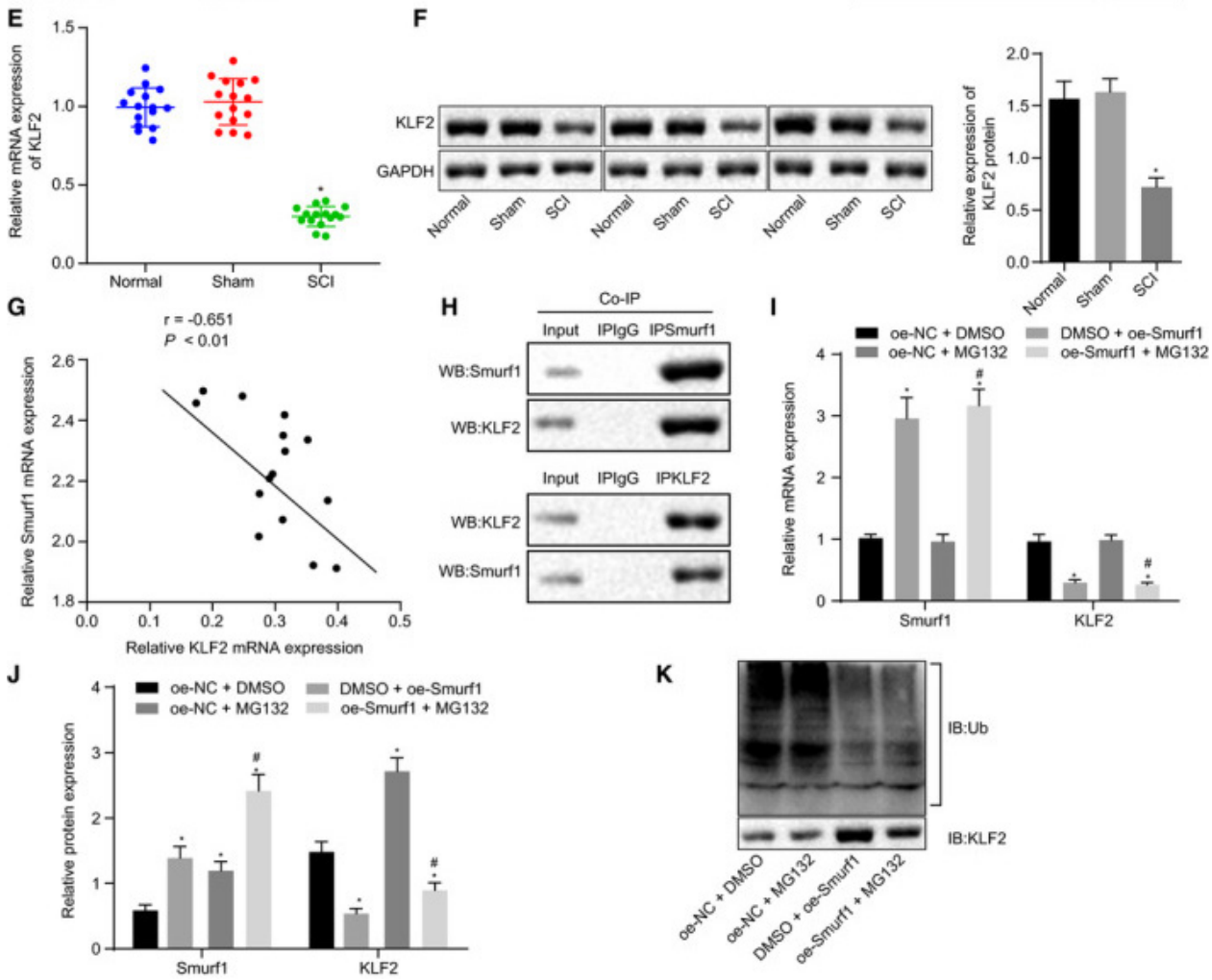

Smurf1 degrades KLF2 via its E3 ubiquitin ligase function. (E) The expression of KLF2 mRNA in the spinal cord of rats after modelling detected by RT-qPCR normalized to GAPDH. (F) The expression of KLF2 protein in the spinal cord of rats after modelling detected by Western blot analysis normalized to GAPDH. (G) The correlation between the expression of KLF2 and Smurf1 in SCI rats analysed by Pearson's correlation analysis (n = 15). (H) The interaction between Smurf1 and KLF2 verified by the Co-IP experiment. (I) mRNA expression of Smurf1 and KLF2 in the transfected cells detected by RT-qPCR normalized to GAPDH. (J) The expressions of Smurf1 and KLF2 protein in transfected cells detected by Western blot analysis normalized to GAPDH. (K) The transfer of Ub molecule by KLF2 in transfected cells detected by Western blot analysis normalized to GAPDH. *P < .05 vs sham-operated rats and normal rats, or the treatment with oe-NC + DMSO, #P < .05 vs treatment with oe-NC + MG132. Comparisons among multiple groups were performed with one-way ANOVA. Pearson's correlation analysis was conducted for the relationship between KLF2 and Smurf1. Rats: n = 15 in each group. The cell experiments were repeated 3 times.

Figure 5

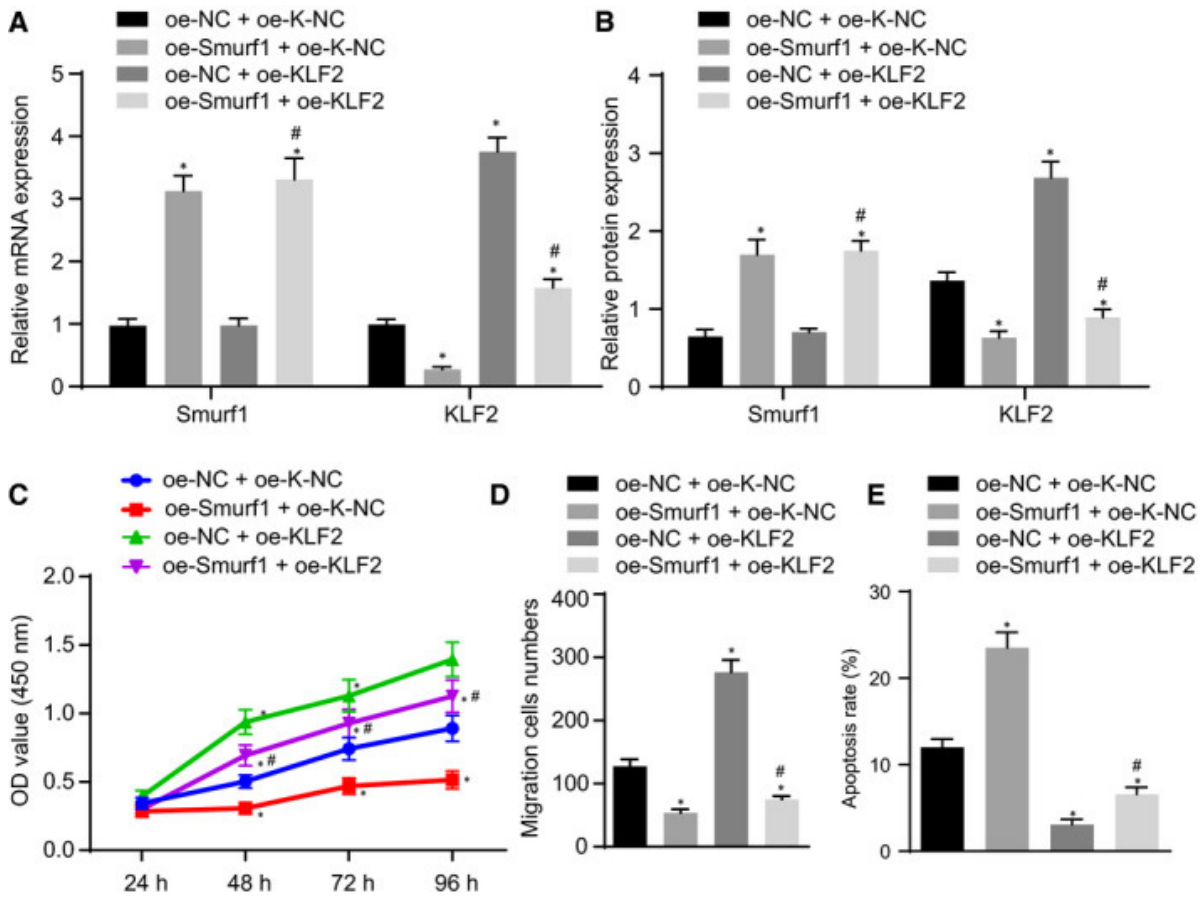

Overexpression of Smurf1 promotes KLF2 degradation to induce apoptosis, but represses proliferation and migration in NSCs. NSCs were transfected with oe-NC + oe-K-NC, oe-Smurf1 + oe-K-NC, oe-NC + oe-KLF2 and oe-Smurf1 + oe-KLF2. (A) The mRNA expression of Smurf1 and KLF2 in NSCs measured by RT-qPCR normalized to GAPDH. (B) Expressions of Smurf1 and KLF2 protein in NSCs detected by Western blot analysis normalized to GAPDH. (C) NSC viability measured by CCK-8. (D) NSC migration evaluated by Transwell assay. (E) NSC apoptosis assessed by flow cytometry using a Bio-Rad ZE5 Cell Analyzer. *P < .05 vs NSCs transfected with oe-NC + oe-K-NC, #P < .05 vs NSCs transfected with oe-NC + oe-KLF2. Comparisons among multiple groups were performed with one-way ANOVA and cell viability at different time-points was compared using two-way ANOVA. The cell experiment was repeated 3 times.

Smurf1 inhibited proliferation and migration and promoted apoptosis of NSCs by promoting the degradation of KLF2

To explore the interaction between Smurf1 and KLF2, both were overexpressed in NSCs. Results from RT-qPCR and Western blot analysis showed that Smurf1 overexpression increased Smurf1 levels but decreased KLF2 levels, while KLF2 overexpression did not affect Smurf1 levels (Figure 5). Co-overexpression of Smurf1 and KLF2 elevated Smurf1 but reduced KLF2. Functionally, Smurf1 overexpression decreased NSC viability and migration while increasing apoptosis. Conversely, KLF2 overexpression enhanced viability and migration and reduced apoptosis. These results indicated that Smurf1 induced apoptosis but repressed the proliferation and migration abilities in NSCs by degrading KLF2.

KLF2 inhibited the expression of ATF2 to promote proliferation and migration but suppress apoptosis in NSCs

ATF2, identified by GeneCards database as a transcription factor binding to the KLF2 gene promoter, was found to be significantly up-regulated in SCI rats compared to normal and sham-operated rats (Figure 6). A negative correlation between KLF2 and ATF2 expression was observed in SCI rats. Overexpression experiments in NSCs showed that up-regulating KLF2 increased its expression but decreased ATF2, while overexpressing ATF2 did not affect KLF2 but increased ATF2. KLF2 up-regulation enhanced NSC viability and migration and inhibited apoptosis, effects that were reversed by ATF2 overexpression. Overall, KLF2 promotes NSC proliferation and migration by down-regulating ATF2.

Figure 6

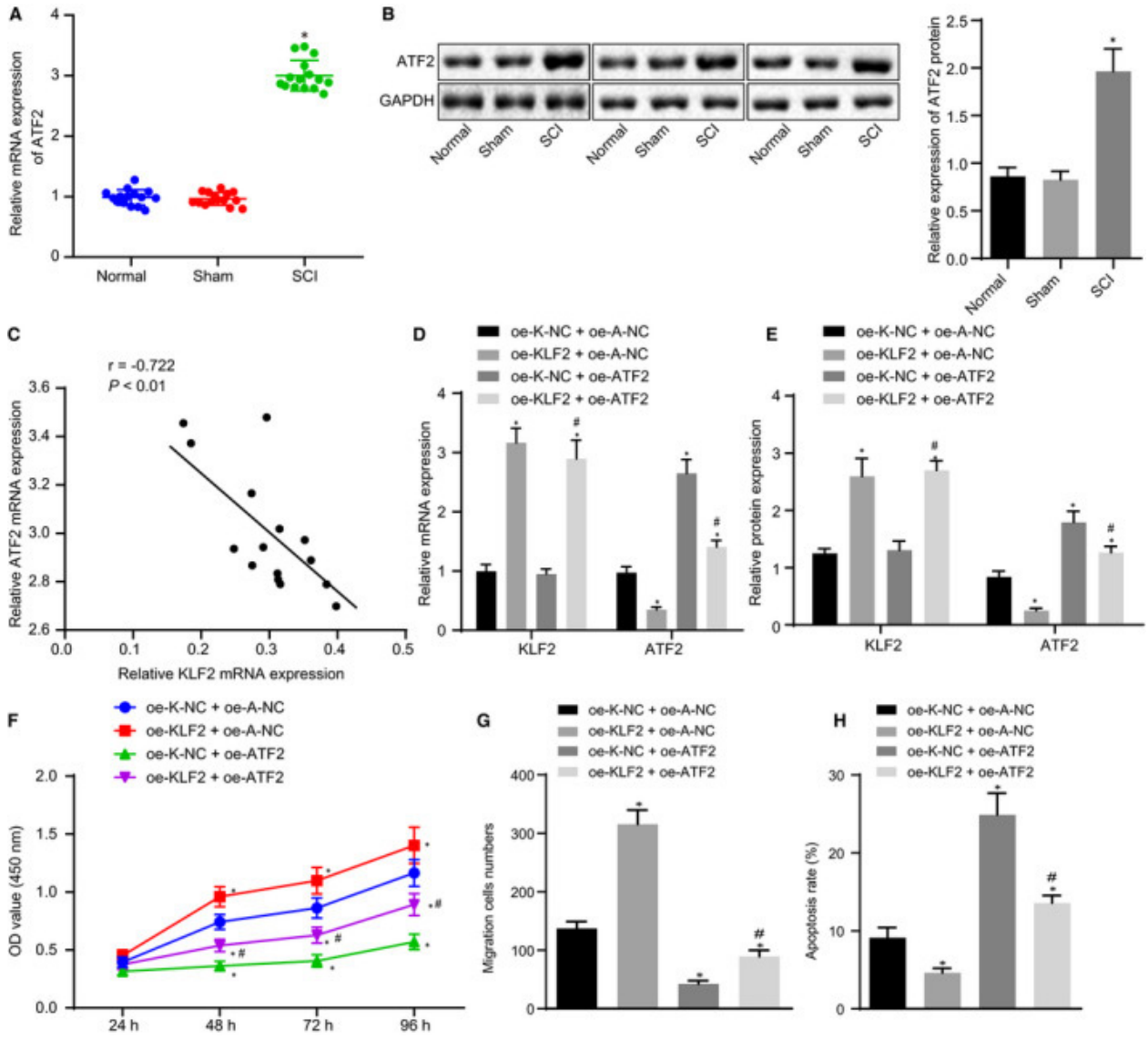

The overexpression of KLF2 down-regulates ATF2 to induce proliferation and migration but represses apoptosis in NSCs. (A) Expression of ATF2 mRNA in the spinal cord of rats after modelling detected by RT-qPCR normalized to GAPDH. (B) Expression of ATF2 protein in the spinal cord of rats after modelling detected by Western blot analysis normalized to GAPDH. (C) Correlation between the expressions of KLF2 and ATF in SCI rats analysed by Pearson's correlation analysis (n = 15). NSCs were transfected with oe-K-NC + oe-A-NC, oe-KLF2 + oe-A-NC, oe-K-NC + oe-ATF2 and oe-KLF2 + oe-ATF2. (D) ATF2 and KLF2 mRNA expression in NSCs measured by RT-qPCR normalized to GAPDH. (E) Expressions of ATF2 and KLF2 protein in NSCs detected by Western blot analysis normalized to GAPDH. (F) NSC viability measured by CCK-8. (G) NSC migration evaluated by Transwell assay. (H) NSC apoptosis assessed by flow cytometry on a Bio-Rad ZE5 Cell Analyzer. *P < .05 vs normal rats and sham-operated rats, NSCs transfected with oe-K-NC + oe-A-NC, #P < .05 vs NSCs transfected with oe-K-NC + oe-ATF2. Comparisons among multiple groups were performed with one-way ANOVA, and cell viability at different time-points was compared using two-way ANOVA. Pearson's correlation analysis was conducted for the relationship between KLF2 and Smurf1. Rats: n = 15 in each group. The cell experiment was repeated 3 times.

Smurf1 inhibits the recovery of neurological function after SCI in rats by promoting the degradation of KLF2 and up-regulating ATF2

The effects of the Smurf1/KLF2/ATF2 axis on SCI and neurological recovery can be described as follows. Smurf1 promotes the degradation of KLF2, leading to increased ATF2 expression (Figure 7). RT-qPCR confirmed that sh-ATF2#1 had the highest efficiency in silencing ATF2. In SCI rats, Smurf1 overexpression coupled with ATF2 silencing showed that silencing ATF2 improved BBB scores and reduced pathological injury and apoptosis. However, these improvements were reversed by overexpressing Smurf1. ATF2 silencing decreased ATF2 levels and improved neural marker expression, while Smurf1 overexpression upregulated ATF2 and suppressed KLF2, negating these benefits. Overall, Smurf1 overexpression degrades KLF2, upregulates ATF2, and exacerbates SCI, inhibiting neural function recovery.

Figure 7

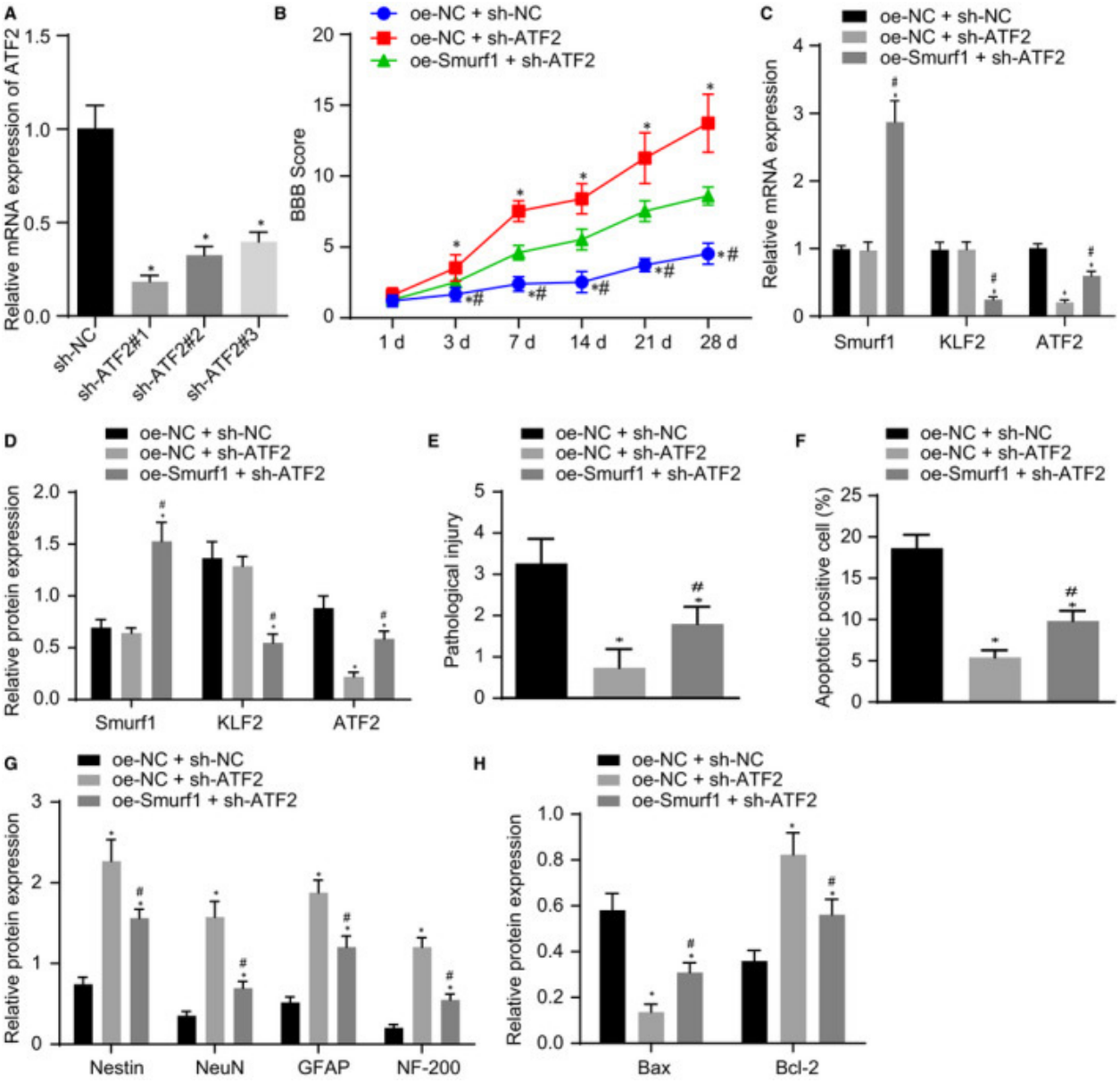

Smurf1 up-regulation activates ATF2 by promoting KLF2 degradation to promote SCI and inhibit the recovery of neural function in SCI rats. (A) Screening of the highest silencing efficacy of ATF2 by RT-qPCR normalized to GAPDH. SCI rats were treated with oe-NC + sh-NC, oe-NC + sh-ATF2 and oe-Smurf1 + sh-ATF2. (B) BBB score of SCI rats. C, RT-qPCR detection of the mRNA expression of Smurf1, KLF2 and ATF2 in the injured spinal cord of rats normalized to GAPDH. (D) Western blot analysis of the protein expression of Smurf1, KLF2 and ATF2 in the injured spinal cord of SCI rats normalized to GAPDH. (E) HE staining analysis of the pathological changes of the spinal cord of rats. (F) Apoptosis cells in the spinal cord of rats detected by TUNEL staining. (G) Western blot analysis of protein expression of Nestin, NeuN, GFAP and NF-200 normalized to GAPDH. (H) The expression patterns of Bax and Bcl-2 protein detected by Western blot analysis normalized to GAPDH. *P < .05 vs SCI rats treated with oe-NC + sh-NC, #P < .05 vs SCI rats treated with oe-NC + sh-ATF2. Comparisons among multiple groups were performed with one-way ANOVA and data at different time-points was compared using repeated-measures ANOVA. Rats: n = 15 in each group.

Up-regulation of miR-125b promoted the recovery of neurological function in SCI rats via Smurf1/KLF2/ATF2 axis

This section describes studies that explored how miR-125b affects the Smurf1/KLF2/ATF2 axis in SCI recovery. miR 125b and ATF2 were overexpressed in SCI rats to assess their effects. miR-125b agomir treatment significantly improved BBB scores and reduced pathological injury and apoptosis, while overexpression of ATF2 worsened these outcomes (Figure 8). However, the addition of miR-125b agomir reversed the detrimental effects of ATF2 overexpression. RT-qPCR and Western blot analyses showed that miR-125b and KLF2 expression increased, whereas Smurf1 and ATF2 decreased in miR-125b-treated rats. Conversely, ATF2 overexpression alone elevated ATF2 but did not affect miR-125b, Smurf1, or KLF2. Furthermore, miR-125b enhanced neural markers like Nestin and GFAP and reduced apoptosis, indicating that miR-125b modulates the Smurf1/KLF2/ATF2 axis, promoting neural recovery in SCI rats.

Figure 8

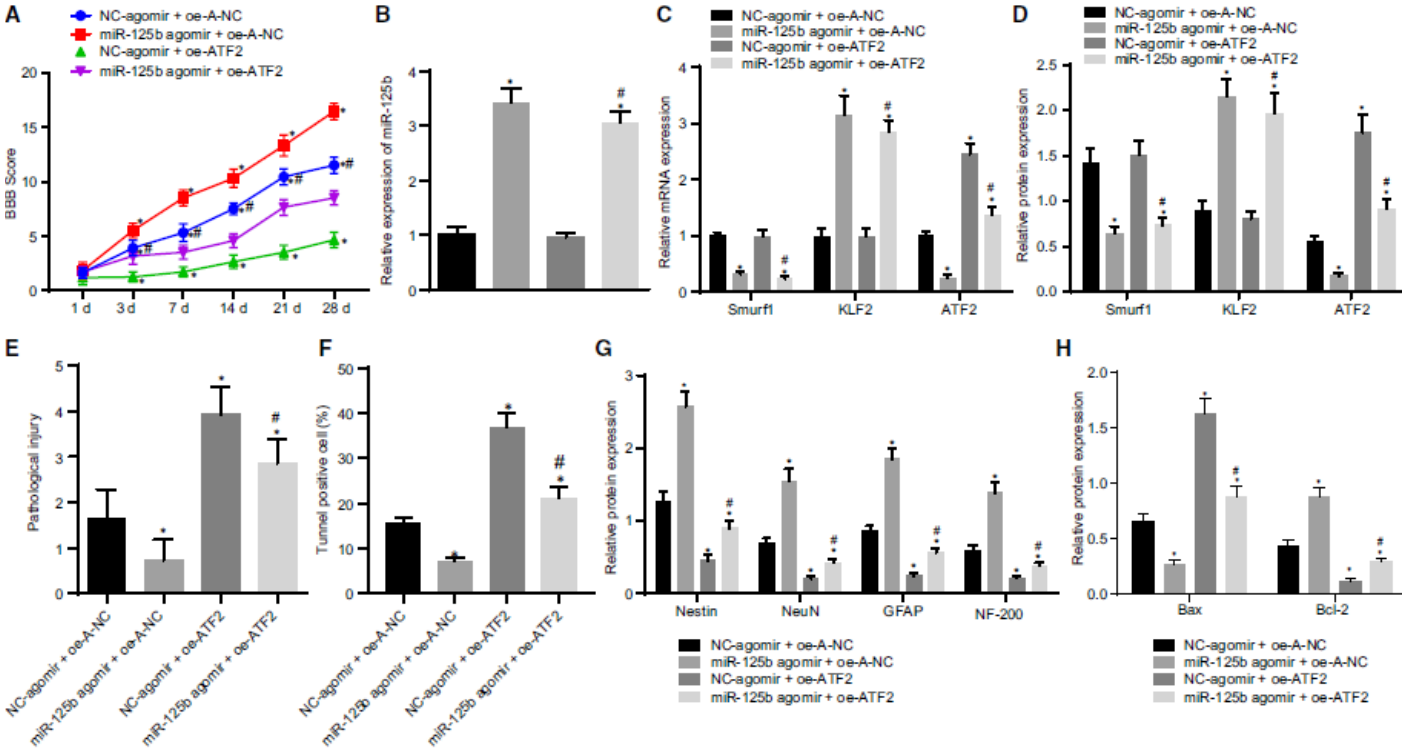

miR-125b modulates the Smurf1/KLF2/ATF2 axis to repress SCI and induce the recovery of neural function in SCI rats. SCI rats were treated with NC-agomir + oe-A-NC, miR-125b agomir + oe-A-NC, NC-agomir + oe-ATF2 and miR-125b agomir + oe-ATF2. (A) BBB score of SCI rats. (B) RT-qPCR detection of miR-125b expression in the injured spinal cord of rats normalized to U6. (C) RT-qPCR detection of Smurf1, KLF2 and ATF2 mRNA expression in the injured spinal cord of rats normalized to GAPDH. (D) Western blot analysis of Smurf1, KLF2 and ATF2 protein expression in the injured spinal cord of SCI rats normalized to GAPDH. (E) HE staining analysis of the pathological changes of the spinal cord of rats. (F). Apoptotic cells in the spinal cord of rats detected by TUNEL staining. (G) Western blot analysis of protein expression of Nestin, NeuN, GFAP and NF-200 normalized to GAPDH. (H) The expression patterns of Bax and Bcl-2 protein detected by Western blot analysis normalized to GAPDH. *P < .05 vs SCI rats treated with NC-agomir + oe-A-NC, #P < .05 vs SCI rats treated with NC agomir + oe-ATF2. Comparisons among multiple groups were performed with one-way ANOVA and data at different time-points was compared using repeated-measures ANOVA. Rats: n = 15 in each group.

Discussion

This study explored the role of miR-125b in SCI recovery, focusing on its regulation of the Smurf1/KLF2/ATF2 axis. miR-125b is known to mediate various neurobiological processes and has shown potential in promoting neurological recovery. The authors found that miR-125b up-regulates KLF2 by targeting Smurf1, leading to reduced ATF2 levels and enhanced neurological recovery in SCI rats. Initially, SCI rats exhibited down-regulated miR-125b and KLF2, and up-regulated Smurf1 and ATF2. Manipulating these factors (overexpressing miR-125b or KLF2, silencing Smurf1 or ATF2) improved neural function and reduced apoptosis.

The study confirmed that miR-125b targets Smurf1, which normally degrades KLF2, a repressor of ATF2. By modulating this pathway, miR-125b promoted the proliferation, differentiation, and migration of NSCs while inhibiting apoptosis. These findings align with previous research indicating miR-125b's role in reducing neuroinflammation and apoptosis in other neurological contexts.

Despite promising results, the study highlights limitations, such as the complexity of miRNA interactions and the need for further research to translate animal model findings to human clinical applications. Moreover, the focus on NSCs, while insightful, necessitates additional investigation into spinal cord neurons, which are central to SCI-induced neurological dysfunction.

Overall, miR-125b shows potential as a therapeutic target for SCI by enhancing neurological recovery through the Smurf1/KLF2/ATF2 axis, but comprehensive strategies and further human studies are required to fully assess its clinical applicability.

Flow Cytometry

Can Rare Event Analysis Ever be High-Throughput?

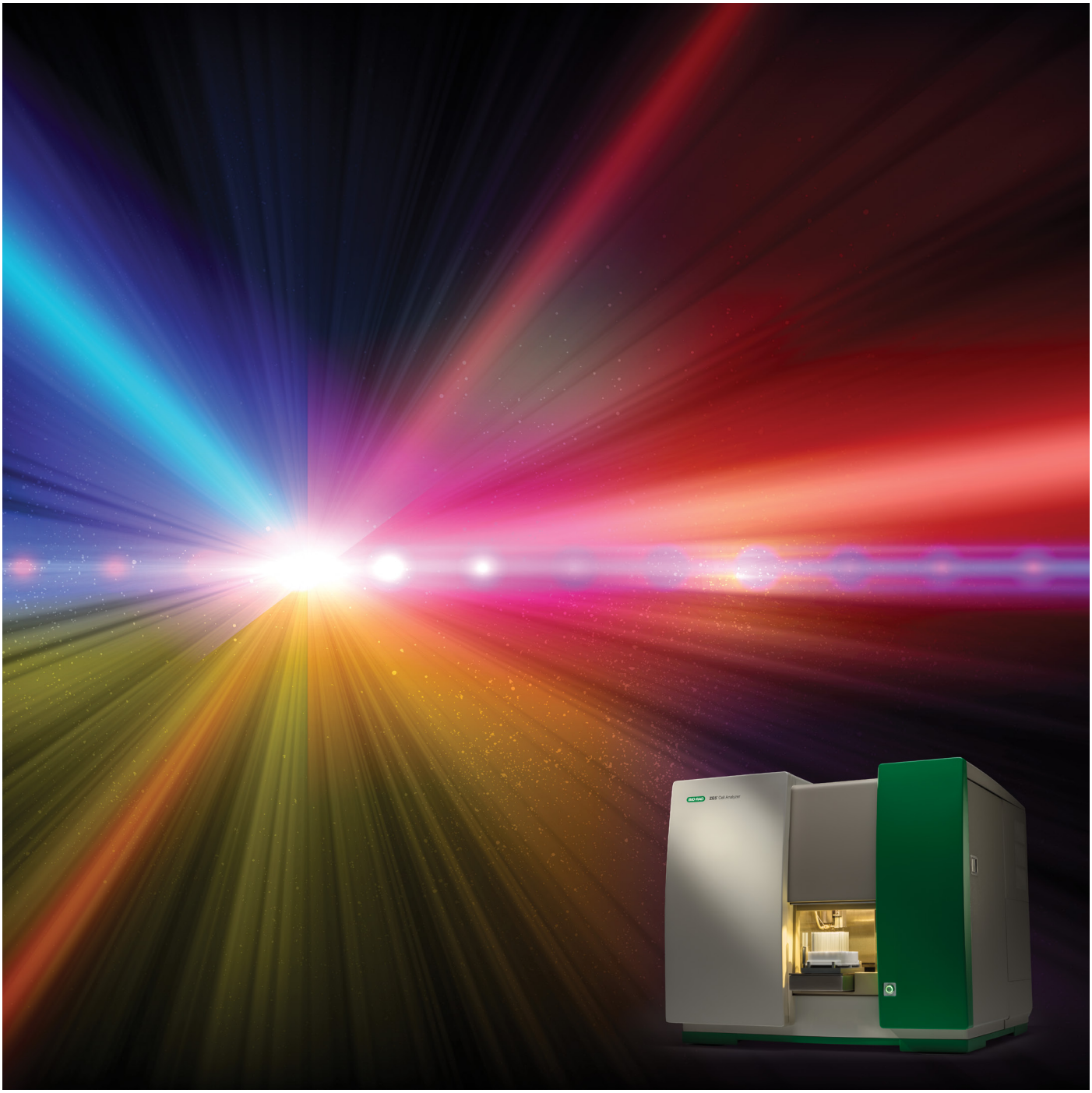

Visit **bio-rad.com/ze5** to find out more about the ZE5 Cell Analyzer.

BIO-RAD

Flow Cytometry

We are all familiar with the idea that time is needed to accomplish great things. Everyone knows that "Rome wasn't built in a day" and "You can't rush perfection". There are activities in research that fall into this category too. PhDs cannot be accomplished overnight, a one-hour incubation cannot be completed in five minutes and a well-written manuscript takes time to perfect, ChatGPT notwithstanding. So what about rare event analysis in flow cytometry? Can it be done quickly? And can it ever be amenable to high-throughput? We set out to test how quickly the ZE5 Cell Analyzer can perform rare event analysis and how that performance can be leveraged for high-throughput assays.

Applications that rely on the detection of rare events, such as stem cell analysis, often require a large number of total events to be acquired in order to detect a much smaller number of rare events. Therefore, the more events that can be captured in a given amount of time the better. Importantly, any data loss in the form of electronic aborts or loss of data resolution is detrimental and, at worst, invalidating.

By using a serial dilution of beads, we found that the ZE5 Cell Analyzer maintained a 1:1 ratio between the observed event rate and the expected event at all event rates up to 100,000 events/second. In other cytometers tested, the observed event rate began to drop below the expected event rate at approximately 20,000 events/second (Figure 1A). Even at this incredibly high event rate, there was no significant change in data spread due to the increased acquisition rate (Figure 1B). To illustrate the amount of time that can be saved by using a high event rate in rare cell analysis, 40 million cells were collected from a single sample. This is equivalent to collecting 400 rare cells at a frequency of 1:100,000. At 20,000 events/second (equivalent to a data rate achievable with competitor instruments without losing data) acquisition took approximately 50 minutes. At 100,000 events/second, acquisition took less than 10 minutes (Figure 1C).

We have proved that the ZE5 Cell Analyzer can process individual samples quickly. But this by itself does not satisfy our question of "can rare event analysis be high-throughput?". To show that a high event rate can be combined with high-throughput, we aimed to demonstrate that 100,000 cells or more can be collected from each well of a 96-well plate with a total analysis time of less than 15 minutes. Alternate columns of a 96-well plate were loaded with Ramos cells. Odd numbered columns were loaded with 100% unlabeled cells, even numbered columns were loaded with 50% unlabeled cells plus 50% labeled cells. All events over the threshold were considered to be cells (Figure 2A). Doublet exclusion was performed (Figure 2B) followed by identification of positive cells (Figure 2C).

The total number of cells analyzed in each well exceeded the target of 100,000 cells/well (mean=116,144, SD=18,280 cells). In even numbered wells, an accurate 1:1 ratio was confirmed (mean=50.8%, SD=0.87%, Figure 2D). The carryover of positive cells measured in odd numbered wells was remarkably low (mean=23, SD=17 cells, Figure 2E). There is no clear correlation between analysis order and rate of carryover (Figure 2E). Total analysis time for the whole plate was <15 minutes.

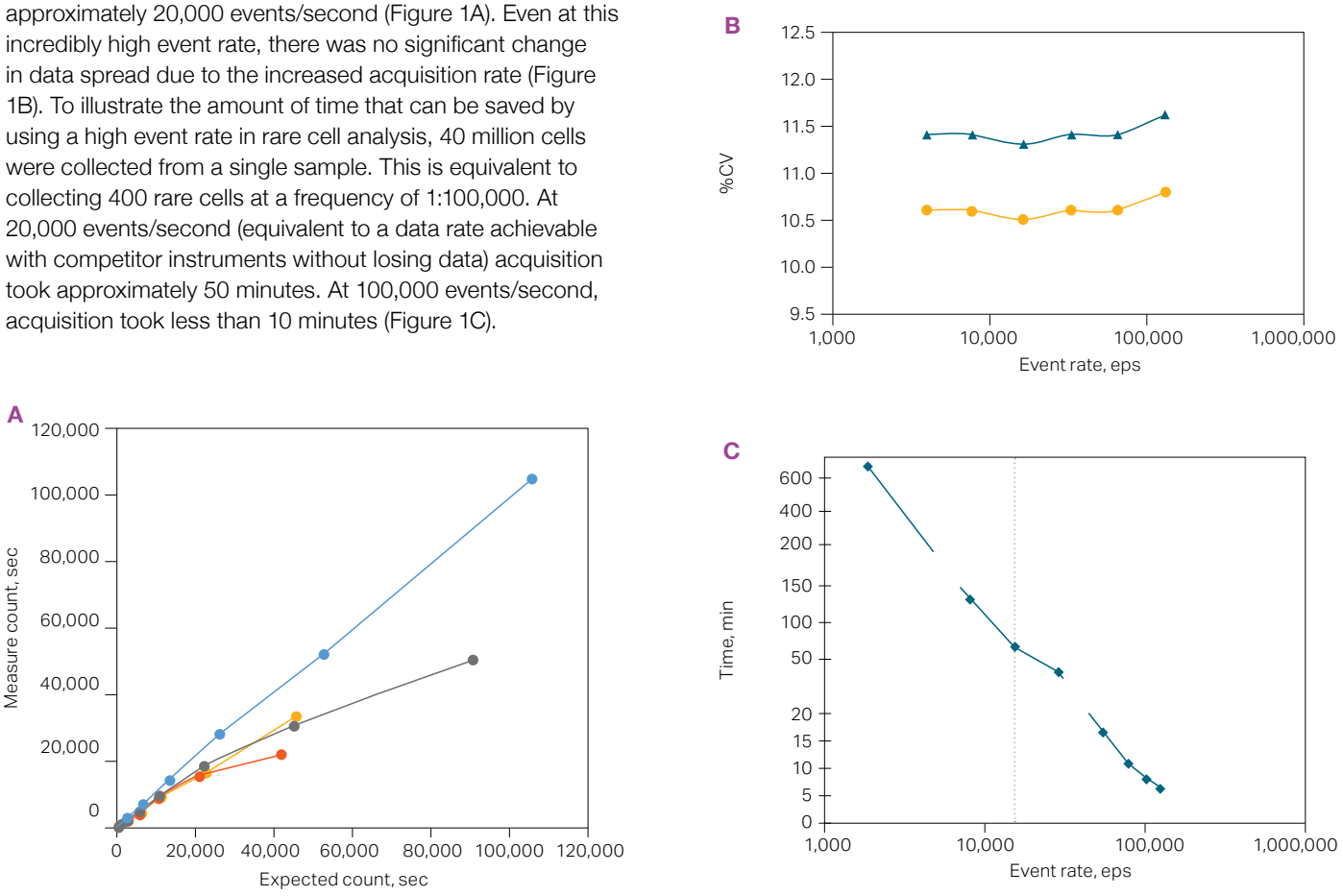

Figure 1: Acquisition rate demonstration on single samples

Flow Cytometry

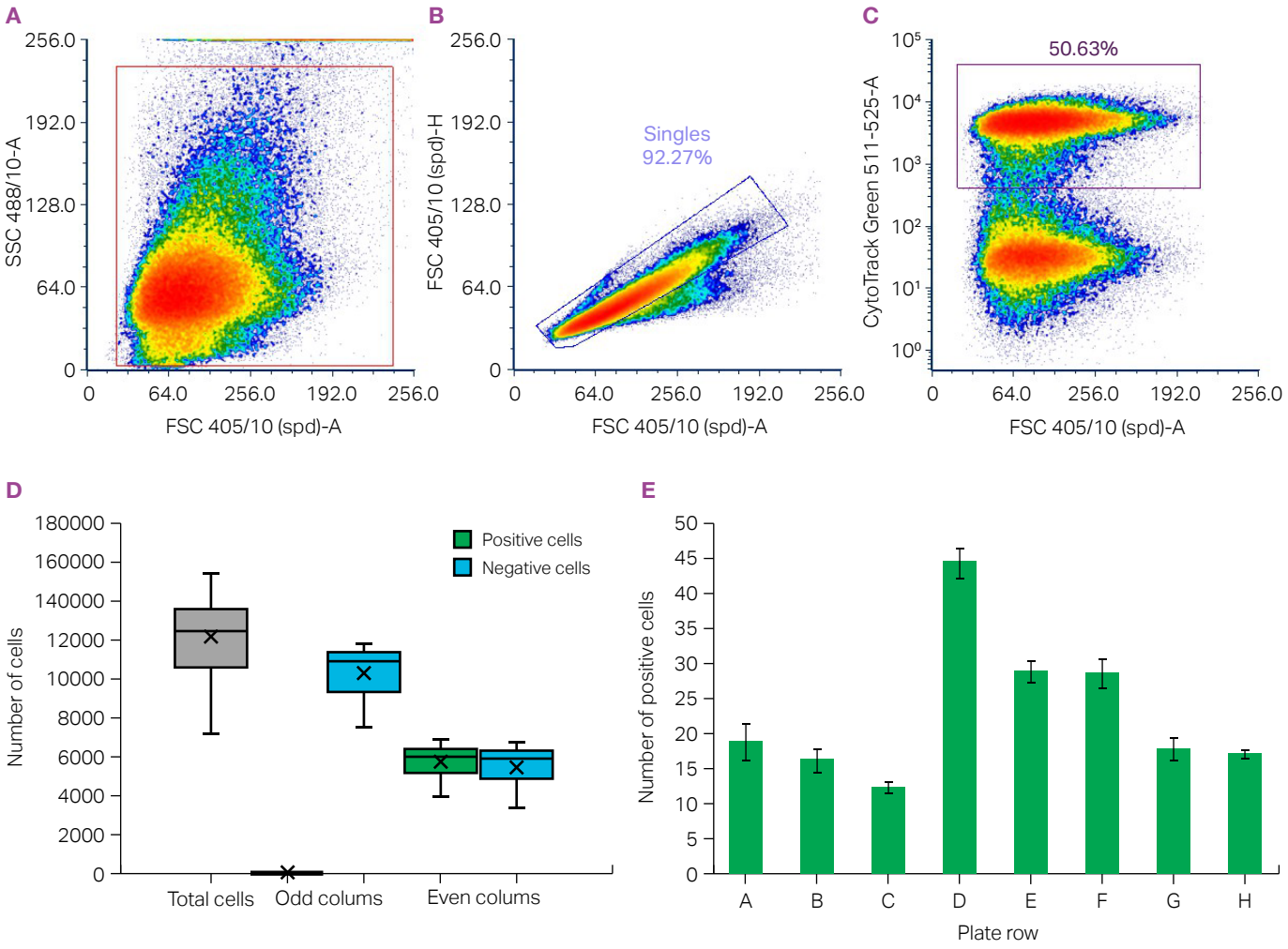

Figure 2: Data acquisition at high event rate over a full 96 well plate

While it is true that 100,000 events from a single well may not always be sufficient for rare event analysis, it nonetheless demonstrates the possibilities of combining a high event rate with high-throughput analysis. The ZE5 Cell Analyzer also features an integrated and fully programmable plate shaker as well as plate temperature control and automatic shut-down and cleaning for extended acquisition runs. For even greater throughput its advanced API facilitates automation with any integration provider.

Of course, there will always be a time component to rare event analysis. But just as modern building techniques have vastly increased what is achievable in a day with far less labor, even in Rome, a modern flow cytometer like the ZE5 Cell Analyzer can vastly increase what you can achieve in your day.

Visit **bio-rad.com/ze5** to find out more about the ZE5 Cell Analyzer.

BIO-RAD

Flow Cytometry

The ZE5 Cell Analyzer in Stem Cell Research

The following publications represent a snapshot of scientific publications published between 2022 and 2023 in the field of stem cell research. All publications utilized the ZE5 Cell Analyzer.

Genome-Wide Association Study on 13,167 Individuals Identifies Regulators of Blood CD34+ Cell Levels

Lopez de Lapuente Portilla A et al. (2022). **Blood** 139, 1659-1669.

Brief Summary

Hematopoietic stem cell (HSC) transplantation is a well-accepted therapeutic strategy in the treatment of blood malignancies. The most commonly used method to harvest HSCs is to stimulate their mobilization from the bone marrow into the blood, followed by leukapheresis. The authors of this study used a combination of genotyping, association analysis, and flow cytometry phenotyping to identify genetic factors that control blood CD34+ cell levels. They identified nine significant and two suggestive associations. Most notably four mapped to CXCR4, already known to be an important regulator of HSC and progenitor cell mobilization. The most significant association mapped to PPM1H a gene not previously implicated in HSC and progenitor cell biology, leading the authors to suggest PPM1H as a potential inhibition target for stem cell mobilization.

The ZE5 Cell Analyzer played an essential role in phenotyping and quantifying CD34+ cells in this sizable dataset. This paper highlights the ability of the ZE5 Cell Analyzer to acquire a large number of cells (up to one million per sample) from an extensive patient cohort. This study shows how the high event rate achievable with the ZE5 Cell Analyzer can benefit this type of application.

Flow Cytometry

Motixafortide and G-CSF to Mobilize Hematopoietic Stem Cells for Autologous Transplantation in Multiple Myeloma: A Randomized Phase 3 Trial

Crees ZD et al. (2023). **Nat Med** 29, 869-879.

Brief Summary

Autologous hematopoietic stem cell transplantation improves survival in multiple myeloma. Using granulocyte colony stimulating factor (G-CSF) alone to stimulate hematopoietic stem and progenitor cell (HSPC) mobilization is suboptimal in many cases. This report of a prospective phase 3 trial focused on the effectiveness of a novel CXCR4 inhibitor, motixafortide, in combination with G-CSF to mobilize HSPCs. The primary endpoint was achieved by 92.5% of individuals and 88.8% met the secondary endpoint, both with a high level of significance over the G-CSF/placebo control.

The ZE5 Cell Analyzer was used to quantify the numbers and proportions of nine individual CD34+ HSPC subsets in 48 patients following HSPC mobilization. The authors used t-distributed stochastic neighbour embedding (t-SNE) projection to display the merged flow cytometry data. Flow cytometry was also used to examine CXCR4 expression on CD34+ HSPC subsets as measured by two monoclonal antibodies recognizing CXCR4 in day one apheresis products from treatment groups.

Flow Cytometry

The Effect of TLR3 Priming Conditions on MSC Immunosuppressive Properties

Tolstova T et al. (2023). **Stem Cell Res Ther** 14, 344

Brief Summary

This study aims to describe optimal priming conditions needed to maximize the immunosuppressive effects of mesenchymal stromal cells (MSCs). Adipose tissue-derived MSCs were expanded and their identity was verified based on cell surface marker expression and differentiation potential. MSCs were then primed by incubation with TLR3 agonist and their immunosuppressive potential was assessed based on their ability to secrete immunomodulatory cytokines. The authors also used a coculture model to assess the effectiveness of MSC-mediated T cell immunosuppression following T cell stimulation with adjuvant. This was based on the observed ability of MSCs to inhibit T cell proliferation and drive apoptosis. The authors conclude that preconditioning MSCs with 10 µg/ml TLR agonist poly(I:C) for 3 hours led to a maximal effect on the secretion of cytokines and this preconditioning regime caused a significant reduction in T cell proliferation, and increased apoptosis.

The ZE5 Cell Analyzer was used for multiple assays throughout this study. Highlighting the flexibility of this technology, it was used to phenotype MSCs and confirm their identity, measure apoptosis, and perform cell cycle analysis. The authors used a combination of propidium iodide and annexin V staining to assess T cell apoptosis following incubation with MSCs. Cell cycle analysis was assessed by the measurement of 5-ethynyl-2'-deoxyuridine (EdU) fluorescence intensity.

Further reading and resources

Aikins ME *et al.* (2022).
Cancer stem cell antigen nanodisc cocktail elicits anti-tumor immune responses in melanoma.
J Control Release 351, 872-882.

Augimeri G *et al.* (2023).
A hybrid breast cancer/mesenchymal stem cell population enhances chemoresistance and metastasis.
JCI Insight 8, e164216.

Bealer E *et al.* (2023).
Extrahepatic transplantation of 3D cultured stem cell—derived islet organoids on microporous scaffolds.
Biomater Sci 11, 3645-3655.

Chen YH *et al.* (2023).
Rewilding of laboratory mice enhances granulopoiesis and immunity through intestinal fungal colonization.
Sci Immunol 8, eadd6910.

Crees ZD *et al.* (2023).
Motixafortide and G-CSF to mobilize hematopoietic stem cells for autologous transplantation in multiple myeloma: A randomized phase 3 trial. Nat Med 29, 869-879.

Harper TC *et al.* (2023).
GATA1 deletion in human pluripotent stem cells increases differentiation yield and maturity of neutrophils.
iScience 26, 107804.

Kang YA *et al.* (2023).
Secretory MPP3 reinforce myeloid differentiation trajectory and amplify myeloid cell production.
J Exp Med 220, e20230088.

Larouche JA *et al.* (2023).
Spatiotemporal mapping of immune and stem cell dysregulation after volumetric muscle loss.
JCI Insight 8, e162835.

Leclerc K *et al.* (2023).
Hox genes are crucial regulators of periosteal stem cell identity.
Development 150, dev201391.

Lee JS *et al.* (2022).
The insulin and IGF signaling pathway sustains breast cancer stem cells by IRS2/PI3K-mediated regulation of MYC. Cell Rep 41, 111759.

Li F *et al.* (2022).
Fas ligand-modified scaffolds protect stem cell derived 13-cells by modulating immune cell numbers and polarization.
ACS Appl Mater Interfaces 15, 50549-50559.

Lopez de Lapuente Portilla A *et al.* (2022).
Genome-wide association study on 13,167 individuals identifies regulators of blood CD34+cell levels.
Blood 139, 1659-1669.

Otsuka T *et al.* (2022).
Overexpression of NDST1 attenuates fibrotic response in murine adipose-derived stem cells.
Stem Cells Dev 31, 787-798.

Tolstova T *et al.* (2023).
The effect of TLR3 priming conditions on MSC immunosuppressive properties.
Stem Cell Res Ther 14, 344.

Visit bio-rad.com/ZE5 for more information.

WILEY

Imprint

Email: info@wiley-vch.de

Editor: Dr. Christina Poggel

RA45335.728587963